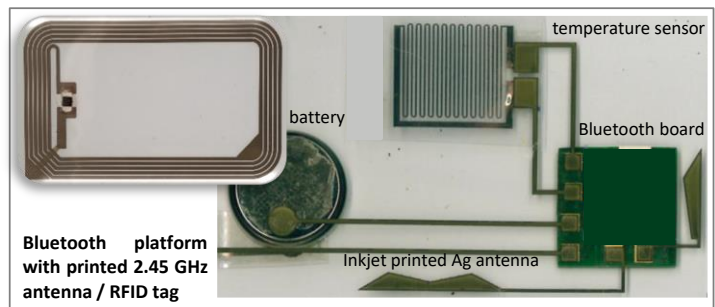
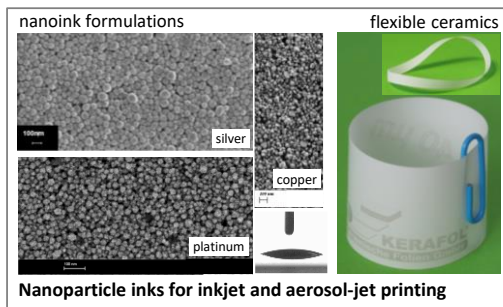
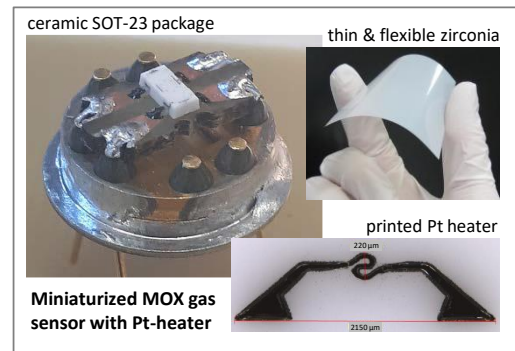
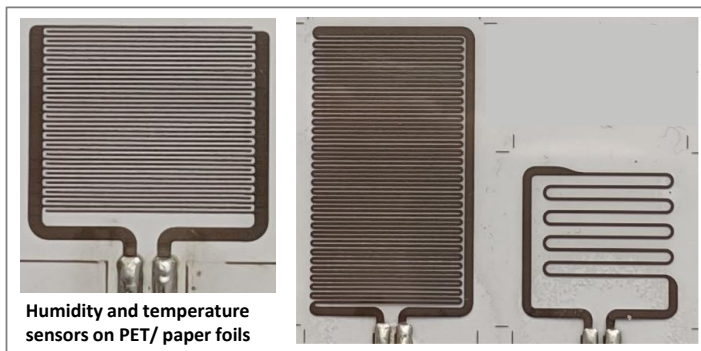


# DIGITAL MANUFACTURING TECHNOLOGIES FOR THE DEVELOPMENT OF SMART SENSORS AND ELECTRONICS FOR AGRO-INDUSTRIAL SYSTEMS





# DIGITAL MANUFACTURING TECHNOLOGIES FOR THE DEVELOPMENT OF SMART SENSORS AND ELECTRONICS FOR AGRO-INDUSTRIAL SYSTEMS

## Research and development report of the MANUNET ERA-NET collaboration project „DigiMan“

Project duration: 01.12.2017 – 30.11.2020

### Main author

Dr. Marco Fritsch  
Fraunhofer IKTS Institute  
Dresden, Germany

### Co-authors

Ayala Kabla (coordinator)  
PV Nano Cell Ltd.  
Migdal Ha'Emek, Israel

Dr. Ralf Zichner | Dana Mitra  
Fraunhofer ENAS Institute  
Chemnitz, Germany

Neil Shaly  
CPC Solutions Ltd.  
Karmiel, Israel

Sunil Kapadia  
Technical University Chemnitz  
Chemnitz, Germany

Lena Wissmeier  
Kerafol GmbH & Co. KG  
Eschenbach, Germany

Dr. Nikolay Samotaev  
Nation Research Nuclear University Mephi  
Moscow, Russia

### Funding information

#### Germany

This research and development project was funded by the German Federal Ministry of Education and Research (BMBF) within the „Innovations for Tomorrow's Production, Services, and Work“ Program (funding number 02P15B520 ff) and implemented by the Project Management Agency Karlsruhe (PTKA).  
The author is responsible for the content of this publication.

SPONSORED BY THE



Federal Ministry  
of Education  
and Research

#### Israel

Sponsored by the Israel Innovation Authority.



רשות החדשנות  
Israel Innovation  
Authority

#### Russia

Sponsored by the Ministry of Science and Higher Education of the Russian Federation founding No. RFMEFI58718X0054.



# Table of contents

<b>1</b>	<b>DigiMan project consortium</b>	<b>6</b>
<b>2</b>	<b>Project summary</b>	<b>7</b>
<b>3</b>	<b>Project motivation and state of the art</b>	<b>8</b>
3.1	Projekt Motivation	8
3.2	State of the art	9
3.2.1	Sensors for smart agriculture	9
3.2.2	Metal oxide gas sensors	10
3.2.3	Printed Sensors on low-cost flexible substrates	11
3.2.4	Nanoinks for direct printing	12
<b>4</b>	<b>Results</b>	<b>13</b>
4.1	Sensor specifications	13
4.1.1	Gas sensor layout and specification	13
4.1.2	Temperature and humidity sensor layout and specification	15
4.1.3	Printed antenna	16
4.2	Material developments	17
4.2.1	Silver and copper inks	17
4.2.2	Platinum ink	20
4.2.3	Gas sensitive materials	23
4.2.4	Thin zirconia substrate	23
4.3	Gas sensor with ceramic membrane and package	25
4.3.1	Printing of platinum heater and sensing electrode	26
4.3.2	Fabrication of ceramic package and sensor assembly	31
4.3.3	Gas sensor testing	34
4.4	Temperature and humidity sensors on foil substrates	38
4.4.1	Printing process development	38
4.4.2	Temperature sensor optimization and testing	40

4.4.3	Humidity sensor optimization and testing	43
4.4.4	Scaling of inkjet printed sensors to R2R	46
4.5	Bluetooth sensor platform and RFID NFC sensor tag with printed antennas for wireless sensor communication	49
<b>5</b>	<b>Project publications</b>	<b>52</b>
<b>6</b>	<b>References</b>	<b>53</b>
<b>7</b>	<b>Tables</b>	<b>55</b>
<b>8</b>	<b>Figures</b>	<b>56</b>

# 1 DigiMan project consortium

The DigiMan project consortium consisted of 7 partners and was coordinated by **PV Nano Cell Ltd.** (Israel). PVN offers complete solutions for mass-produced inkjet based printed electronics. This includes nanoparticle based conductive inks, inkjet production printers and the complete printing process. PVN's solutions are used all over the world in a range of digital printing applications including automotive, IoT, photovoltaics, printed circuit boards, flexible printed circuits, antennas, sensors, heaters and touchscreens.

The German sub-consortium was coordinated by **Fraunhofer Institute for Ceramic Technologies and Systems IKTS** (Germany). IKTS represents Europe's largest R&D service provider dedicated to the study of ceramics and related technologies. The group "Materials for Printed Systems" develops powders and powder suspensions (pastes, slurries and inks) for coating technologies (screen printing, dispensing, inkjet and aerosol printing, tape casting etc.) as well as scientific and engineering knowledge in the field of physical material properties, chemical interactions and high-temperature electrochemistry.

**CPC Solutions Ltd.** (Israel) is specialized in the design, engineering and manufacturing of tailor-made Human Machine Interface (HMI) solutions for commercial and defense applications. CPC offers in-house manufacturing capabilities for printed electronics, SMT assembly and electro-mechanical assembly. With more than 30 years of experience in HMI engineering, CPC is a one-stop partner for HMI hardware.

**KERAFOL Keramische Folien GmbH & Co. KG** (Germany) is a specialist for ceramic tapes and a major manufacturer of technical ceramics. Kerafol develops and manufactures products for thermal management, porous ceramic filters, materials for fuel cells, and ceramic substrates. These are used in a wide variety of applications, such as microelectronics, battery technology, (waste) water filtration, SOFC/SOE, and sensor technology.

The **Fraunhofer Institute for Electronic Nano Systems ENAS** (Germany) is the specialist and development partner in the field of Smart Systems and their integration for various applications. Application areas are semiconductor industry, aeronautics, automotive industry, communication technology, security sector, logistics, agriculture, process technology and medical as well as mechanical engineering. ENAS offers innovation consulting and supports customer projects, starting from the idea, via design and technology development or realization based on established technologies up to tested prototypes.

**Chemnitz University of Technology** (Germany) is a diverse university that is a part of a strong regional, national and international network. It is home to roughly 10,000 students from around 100 countries. The focus of the Institute for Print and Media Technology (pmTUC) is on current developments in the printing and media industry, especially on the promising area of printed electronics.

**National Research Nuclear University MEPhI** (Russia) is a leading Russian University. The "Nanoelectromechanical systems and sensors" laboratory of the Moscow Engineering Physics Institute works on the development of low power and high selective semiconductor metal oxide and field effect gas sensors based on silicon and ceramic technologies and semiconductor physical detectors of nuclear irradiations. In the field of MOX-gas sensors MEPhI cooperates with the company **RIIT Ltd.** (Russia) in the field of sensor development and testing.

## 2 Project summary

The **DigiMan** project developed innovative sensor platforms for **agro-industrial applications** by providing a digital manufacturing process chain based on **printing technologies and nanomaterial inks**. This makes it possible to miniaturize the sensors, to achieve a flexibility in the target sensor properties and to realize these sensors in economically low cost even for small sensor batch quantities.

The project utilized digital technologies for the sensors manufacturing, illustrating the benefits of a 3-D prototype philosophy (rapid, simple and cost effective). Environmentally friendly **digital additive printing technologies** like inkjet or aerosol-jet as well as drop-coating and laser machining made it possible to miniaturize the sensors sizes, along with a reduction in needed sensor power consumption. The applied technologies allow the customization of sensor properties and to realize this economically even for small sensor batch quantities. The equipment involved does not need expensive clean-rooms or vacuum technologies and is already introduced in the market. The software for digital design of manufacturing this sensor platforms is simple and has open access or free distribution on student level, which makes a significant contribution to the dissemination of the developed technologies and materials among future engineers by a reduced “price of entrance”.

Material developments lead to the application of self-synthesized **silver, copper and platinum nanoparticle inks**, which are compatible to inkjet and aerosol-jet printing (particle size control < 200 nm, variation of ink solid content up to 50 wt.-%, good sedimentation stability achieved). These were used for the resource-efficient printing of miniaturized heaters, antennas for wireless data transmission and functional sensor layers to detect humidity and temperature.

The **first sensor platform** comprised a **metal-oxide semiconductor gas sensor** (MOX, ceramic MEMS) printed on a newly developed very thin (20 to 40  $\mu\text{m}$ ) and **mechanically flexible yttria stabilized zirconia membrane**. A direct **printed miniaturized platinum heater** (40  $\mu\text{m}$  line width, up to 500  $^{\circ}\text{C}$  local temperature) led to a very low power consumption (< 200 mW), which is highly attractive for gas sensing applications. The thin zirconia membrane is compatible to laser processing and ceramic packaging technologies, which have potential to obviate some difficulties associated with traditional packaging technologies (integration of filters, printing antennas, holes for gas access to sensors). This approach can become an attractive alternative for small-scale integration of sensor components. For the gas sensing electrode, special **metal oxide inks** for sensing methane, hydrogen, carbon monoxide and ammonia were developed.

The **second sensor platform** comprised digital printed **humidity** (25 to 75 % RH) and **temperature sensors** (10 to 90  $^{\circ}\text{C}$ ) on low-cost **PET polymer and paper foils**. The inkjet printing method was scaled from sheet-to-sheet to a roll-to-roll manufacturing (R2R). A developed **low energy Bluetooth sensor platform** with silver **inkjet printed antenna** demonstrated the wireless communication of the developed sensors within a 50 m radius. An additionally **printed RFID NFC communication tag** can digitally label individual sensors.

Both developed sensor platforms were tested under agro-industrial relevant parameters, especially in a wide spectrum of temperatures and humidity ranges as well as in the presence of agro-industrial gases.

## 3 Project motivation and state of the art

### 3.1 Projekt Motivation

Agriculture and food production are expanding industries with significant environmental and resource impacts. Excessive use of raw materials, fertilizers and pesticides leads to significant environmental impact, such as nitrate polluted groundwater or increased energy consumption and associated CO<sub>2</sub> emissions. Continuous process monitoring in agricultural areas, such as livestock, fish farms, forestry, grain production and gardening, could help and pave the way for "agriculture 4.0" through "smart agriculture". For this purpose a large number of sensors is needed, which collect data of **temperature, humidity** and in particular **concentrations of gases** reliable and location resolved. Established manufacturing technologies for the production of sensors based on photolithography show complex manufacturing steps and require environmentally harmful chemicals.

The objective of the **DigiMan project** was the development of a digital manufacturing process chain based on **printing technologies** and **nanomaterial-based ink formulations** for the development of smart sensors and hybrid electronics in different fields of applications. The project developed **innovative ceramic- and polymer / paper-based sensor platforms** that can be fabricated with environmentally friendly digital additive manufacturing technologies using **inkjet** or **aerosol jet**. This makes it possible to miniaturize the sensors, to achieve a flexibility in the target sensor properties and to realize these sensors in economically low cost even for small sensor batch quantities. Nanomaterial inks can be used for the resource-efficient printing of miniaturized heaters, sensor elements and antennas for wireless data transmission. Such digital based manufacturing technologies of sensor components can be scaled, even without cleanroom environments, to a **roll-to-roll production** (R2R).

The target DigiMan sensors consume significantly less energy during operation and can be used in a resource-efficient manner. The project consortium with partners from Israel, Russia and Germany see the exploitation of the project results in the growth markets of **sensors for "smart agriculture"**, for recycling processes, the printing industry in the field of digital-additive manufacturing of "printed electronics", new material inks and ceramic sensor membranes for "low -power "sensors. The addressed sensor platforms can also be used to expand sensor networks for the Internet of Things.

## 3.2 State of the art

### 3.2.1 Sensors for smart agriculture

**Livestock facilities.** The quality of environmental conditions at livestock facilities plays an important role in assuring health and well-being of the cattle and staff. Environmental conditions such as **air contaminants concentration, temperature, humidity**, air movement speed influence health, functioning, behavior of animal and man and must be monitored and controlled. All kind of disorders are likely to happen in livestock facilities where climatic conditions are not within the optimum limits because of lack of monitoring and control. According to regulations certain gasses concentration should be maintained at specified levels to ensure animal and human safety and provide high farm productivity.

**Ammonia (NH<sub>3</sub>)** - Ammonia is one of the protein metabolism products in animals' organism. If ammonia concentration at livestock facilities gets high, it can lead to high diseases susceptibility and lower weight gains. Major factors that influence the ammonia concentration include the following: stocking density of the livestock, temperature, humidity, air movement distribution, input-exhaust ventilation systems. Filtration, ventilation, landscaping and dietary changes can be used to decrease the ammonia concentration at facilities based on the output of the gas analysis and environmental control system feedback.

**Carbon Dioxide (CO<sub>2</sub>)** – The main sources of carbon dioxide pollution are identified as exhaled breath and heating systems. Carbon dioxide concentration should be also monitored and controlled at levels below 2500 ppm according to EU Directive. Higher concentrations of carbon dioxide can cause lethargic chicks and reduced weight gains and can be even fatal to livestock and employees.

**Carbon Monoxide (CO)** – According to regulations in different countries and expert recommendations, CO levels should be kept at 10-50 ppm, because high levels can be fatal for humans and animals. It must be also considered that animals should take as much oxygen on board as possible, particularly early in their life.

**Fish farming.** Dissolved oxygen level is crucial in providing high yield and well-being of livestock. At low oxygen concentrations (< 4 mg/l) fish can be stressed, stop eating, and even die, sufficiently reducing a farmer's yield. On the other hand, oxygen concentration should be also monitored because oxygen leaks can cause hyperoxia. So constant monitoring oxygen level and injecting the necessary amount of oxygen to keep the optimum concentration is necessary at next-generation agro-industrial complexes.

**Forestry.** Phosphine (PH<sub>3</sub>) is often used to fumigate timber to protect it against insects and diseases. According to regulations requirements timber should be fumigated before exporting to many countries.

**Food storage**, example "**grain storage**". Grain storage is a crucial task because it is related to high concentration of flammable substances, such as grain, at one place. As grain is a living substance and has the ability to "breathe" and emits gasses (carbon dioxide, water and others), it can go bad (rot) or overheat and cause fire, if it is not properly stored. In both cases, a gas-monitoring system can prevent accidents by detecting **pre-emergency situations** or sufficiently reduce grain damage. Fermenting silage produces such gases as CO<sub>2</sub>, NO, NO<sub>2</sub>, N<sub>2</sub>O<sub>4</sub>, besides that stored organic compounds also produce methane. CO<sub>2</sub> concentrations over 400-500 ppm can be harmful to stored grain.

Monitoring and controlling CO<sub>2</sub> level and other mentioned above gases concentration at low levels will provide the necessary safety conditions for personnel and grain stored.

Pre-emergency situations detection is based on concentration monitoring of specific gas-markers that are emitted at first stages of rotting. Hydrogen is such gas-marker. Unlike other gases, hydrogen, because of its volatility, easily flows up the grain elevator column and can be relatively easy detected even at low concentrations with the use of **gas sensors**.

Pre-emergency situation monitoring is usually done with the use of conventional **temperature sensors**, positioned at the central axis of the grain elevator column with a certain pitch. However, because of low thermal conductivity of grain this monitoring method can miss local grain heating, which leads to fires. The gas method ensures monitoring of the whole grain volume and is much cheaper because it is sufficient to use one hydrogen sensor unit instead of dozens of temperature sensors in the temperature monitoring method. In addition to hydrogen sensors carbon dioxide and **water vapor sensors** can be also used to ensure a monitoring of grain state during storage. Systems, based on these sensors should fulfill the requirements of explosion prevention and fire safety for grain storage facilities, have standard outputs for process control systems unified modules and protocols, compatibility with autonomous power sources.

Besides storing processes monitoring these sensor systems can be implemented in the technological processes of loading, transportation and preparation of grain as gas fire alarms, reacting at smoldering of dust that is formed due to grain abrasion. By using dedicated algorithms of separate data processing, it is possible to measure concentrations of hydrogen and CO on one sensor. This is important because CO is also a marker-gas for detecting of organic materials (dust) smoldering. Semiconductive sensors allow selective hydrogen concentration measurement starting from 0.1 ppm and CO – from 1 ppm. Nowadays electrochemical CO sensors are used in most gas fire alarms, but these sensors have high cross sensitivity to hydrogen, which reduces confidence level of smoldering detection. Devices and systems based on these sensors can operate at any dust content and can be installed in any area, including dust-laden places.

### 3.2.2 Metal oxide gas sensors

**Metal oxide gas sensors** (MOX) are an example for rapid prototyping of MEMS in compact packages for surface mount devices (SMD package). The MOX sensor is not only a complex MEMS product, but it has also a complex and specific package. The general construction of the gas-sensitive metal oxide sensor [1] is a combination of the following parts responsible for functionality: (1) **micro-hotplate**, which is responsible for the level of power consumption and parameters of temperature cycling regime of the metal oxide gas sensor, (2) chemical composition of the nanostructured **metal oxide sensitive layer** to the gas, which is responsible for the sensitivity of the sensor to specific gases and (3) **package**, which is responsible for the functional application in which the sensor can be used (for example, by the level of explosion protection or vibration resistance). Despite the existing market of companies with large production of MOX sensors [2-5] for gas analytics, there are not all-encompassing solutions for sensing tasks (breath tests [6], security application [7], food industry [8]). That is why **fast prototyping methods** are becoming relevant, since they allow the production of small sensor lots with **customized design and layout**. The use of flexible prototyping methods for the production of metal oxide sensors offers a deepened system integration at the instrument level as well as reduced production time and cost for specific semi-customer gas analysis device. This approach must be challenged by already existing MEMS solutions, mainly based on silicon clean room technology, which is demonstrated for example in article [9] for a prototype of gas pre-concentrator. The scaled experimental integration of MOX sensor arrays, need the development of an individual plastic package [10]. Larger

serial scale products like Gas Sensor Modules for Indoor Air Quality monitoring, based on MOX sensors in a micro-assembly based on several silicon chips, use a microcontroller for a normalized digital signal [11-12]. These examples illustrate, that gas sensing applications can vary a lot by environmental application conditions, but there is nearly no flexibility to realize adapted prototype sensors in smaller, cost effective numbers.

Regarding smart sensors and electronics for agro-industrial systems, commercially available sensor solutions show drawbacks concerning continuously and cost-efficient measurement as well as long term stability in corrosive gas environments. For these cases, DigiMan partner Mephi developed MOX gas sensors for industrial use under **harsh environmental conditions** [13], where they combine ceramic substrate and packaging materials with **ceramic MEMS technology** [14].

There is the approach to manufacture MOX sensors with 3D prototyping technologies, which presuppose the availability of materials and methods. DigiMan demonstrates that this approach of fast prototyping of MOX sensors is possible and the sensors are comparable in terms of general gas sensing ability to commercial sensors. Monolithic ceramics based on zirconium oxide [15] and aluminum oxide [16] were chosen as a material for MEMS and SMD package, metallization was performed based on platinum [17] and silver [18] ink for aerosol printing, and a gas sensitive MOX layer was synthesis on the basis of tin dioxide [19]. The construction of the sensor was designed based on the concept of finding a balance between the resolution of the used equipment and acceptable thermal characteristics [20].

### 3.2.3 Printed Sensors on low-cost flexible substrates

Nowadays, electronic products are made in industrial environments mainly based on sophisticated multistep photolithographic technologies. These are mature technologies with high yield, accuracy and automatization. However, these technologies are very expensive as well as highly complex due to multiple process steps. In addition, photolithographic processes are not environmentally friendly due to the application of subtractive processes and hazardous waste production. Furthermore, these technologies are not qualified for the efficient manufacturing of customized products, flexible products of larger size and products that have a high product diversity or in general small to medium product series due to the usage of masks.

The trend towards the use of **inexpensive and mechanically flexible single-use sensors** based on **paper and polymer substrates** can only be realized to a limited extent by means of photolithography, as many material and energy-intensive process steps, such as masking, etching and cleaning, are necessary. With the help of **digital printing technologies** such as **inkjet** printing, sensors can be efficiently individualized and applied to large areas, especially with highly productive **roll-to-roll** processes.

**Inkjet printing** is used for the mass printing of graphics or marking of components in the industry on a scaled basis. Printing functional layers is challenging because the printing inks must be compatible with the printhead and long-term functional stable during operation. Since many of the required sensor materials are not yet available in the form of **printing inks**, there are development opportunities here. Research centers at the TU Chemnitz (formerly Prof. Baumann), the Technical Research Center Finland (VTT) but also the Holst Center in the Netherlands have already proven with large EU flagship projects that the scaled and cost-efficient production of printed electronics and sensors using inkjet is possible [21-23].

Overview publications were recently given by Khan et al. [24] on printed flexible and wearable sensors, Xu et al. [25] on "skin-like" flexible sensors for wearable electronics and Takei et al. [26] on sensors based on "electronic skin". These publications emphasize

the potential of printed sensors for medical diagnostics and fitness monitoring. In particular, additive printing techniques, such as inkjet printing, are seen as an economical, cost-efficient process compared to the established thin-film techniques of microelectronics. Here, the necessary manufacturing steps are reduced (no clean room production) and a large-format up to **roll-to-roll production** of sensors, with high throughput at correspondingly low unit prices, is aimed for. **Silver conductive paths** were demonstrated using inkjet printing on polymer films such as polyimide as a temperature sensor [27]. For the digital printing of Ag, Au and CuNi inks for the metallization of polymer films, **photonic sintering** processes, such as flash lamps or laser sintering, are of particular interest [28]. Compared to the known furnace sintering, they offer the possibility of sintering the printed layers in an extremely shortened time (milliseconds). For portable applications, thin, **flexible polymer and paper foils** are viewed as the substrate of choice for body-near and inconspicuous integration in everyday objects. Temperature sensors on flexible foils were recently demonstrated for the temperature control of goods in transport (<https://www.thinfilmsystems.com>) or as a sensor platform with combined pH and temperature sensor in foil technology by company Innome (<https://accensors.com/foliensensor-technolog>).

### 3.2.4 Nanoinks for direct printing

Printed sensors based on **inkjet or aerosol-jet printing** need print-compatible materials for fabrication, particularly those used for printed electrical conductive layers. Different types of conductive inks include colloidal suspensions of metal nanoparticles, nanowires, carbon nanotubes, organometallic compounds in solution and dissolved or dispersed conductive polymers [29, 30]. The inks need to fulfill a range of specifications, like **low viscosity** (5 – 15 cP), surface tension (30 – 40 mNm), **low particles size** (e.g. < 500 nm) and long shelf life with limited particle sedimentation. The inks often contain several constituents such as organic dispersants, adhesion promoters like binders, surfactants, thickeners, stabilizing agents and other additives [31, 32]. The printed films have to show a high conductivity, even after curing at low temperatures (e.g. < 200 °C) if printed on thermal sensitive polymer or paper substrates, a sufficient adhesion and stability against mechanical substrate bending. On the market mainly **silver** and some gold inks are used for printed circuits and electrodes [29, 33-37]. Beside these, there is a need to broaden the range of inkjet or aerosol-jet printable conductive materials suitable for the fabrication of direct **printed sensors**. Great effort is also being made in the synthesis of inks based on non-noble metal nanoparticles (e.g., Cu, Al, Ni), however they face issues in terms of oxidation stability in ink composition and printed films. **Platinum inks** are highly interesting for printed catalytic layers, impedance electrodes or temperature stable heaters under harsh environmental conditions. Even if there is no commercial platinum ink available, first research publications look promising [38, 39].

## 4 Results

### 4.1 Sensor specifications

#### 4.1.1 Gas sensor layout and specification

**Figure 1** shows the process flow for the development of the gas sensor. Starting from the modeling of heat distribution of different micro-hotplate and ceramic packaging layouts, a miniaturized platinum heater as well as a metal oxide functionalized platinum electrode is printed on both sides of a very thin zirconia membrane. This membrane is placed and integrated in a 3D ceramic package, which consists of a top and bottom part, which both are joined and connected with outer driving electronics by using silver ink printed interconnects.

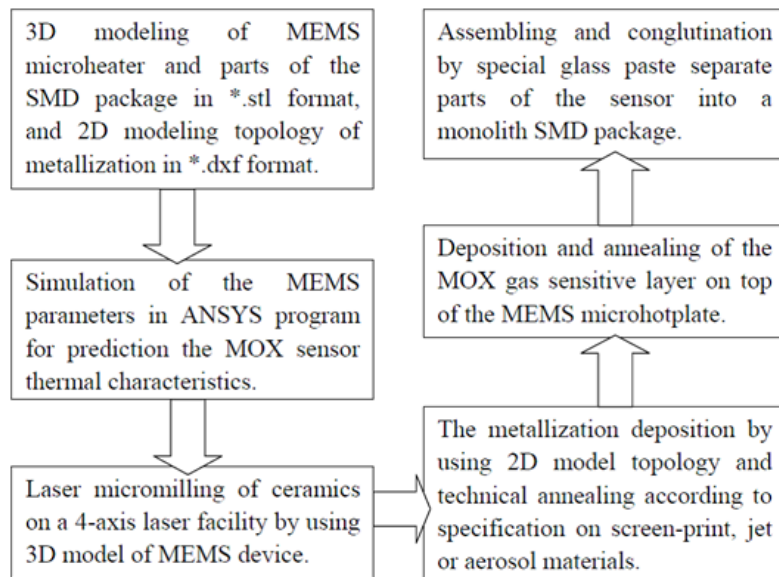


Figure 1: Process flow of gas sensor preparation.

**Table 1** lists the main processing steps for the fabrication of the gas sensor.

Table 1: Steps for the gas sensor fabrication.

Step No.	Processing step	Component
1	Fabrication of thin ceramic membrane	Zirconia membrane with < 40 μm thickness
2	Laser cutting of ceramic membrane	Free cutting of certain membrane areas
3	Printing and annealing of Pt-ink	Pt-heater and Pt-electrodes
4	Micromilling of ceramic packaging substrate	Sensor package top and bottom parts
5	Deposition, annealing of MOX based material	Gas sensitive layer
6	Printing, annealing of Ag metallization	Contact pads on edges of package
7	Gluing ceramic package top to bottom part	Assembling sensor package

**Figure 2** shows the layout of the MOX gas sensor. Since the MOX sensing principle requires a local heating of the gas sensing layer, a miniaturized platinum heater is printed on one side of a thin zirconia membrane. This membrane is very thin (< 40 μm) and shows free-cut areas to reduce the heat dissipation, which makes it possible to run the

“hot-plate” at 400 to 500 °C with very low power consumption < 150 mW. On the other side of the same membrane, platinum electrodes are printed to realize the MOX gas sensitive electrode by coating a gas sensitive material. Finally, this hot-plate membrane “chip” (since it is very small in outer dimension) is integrated in a ceramic sensor package.

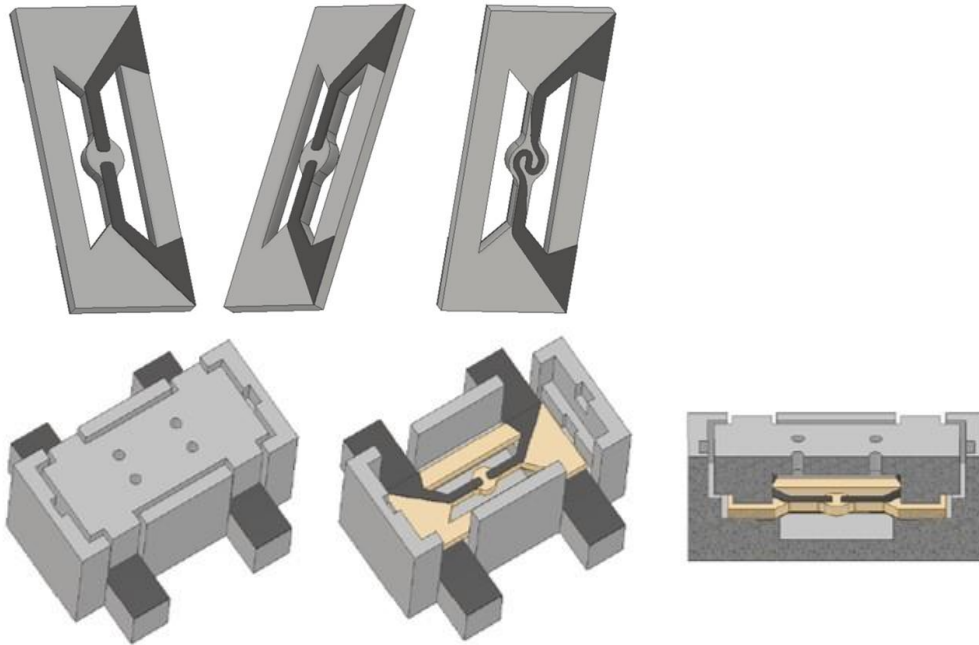


Figure 2: (top) Layout of printed platinum electrode and heater on a thin free-cut zirconia membrane and (bottom) integration of the membrane in a ceramic gas sensor package.

**Figure 3** shows the layout and size of the zirconia membrane and the miniaturized Pt-heater layout.

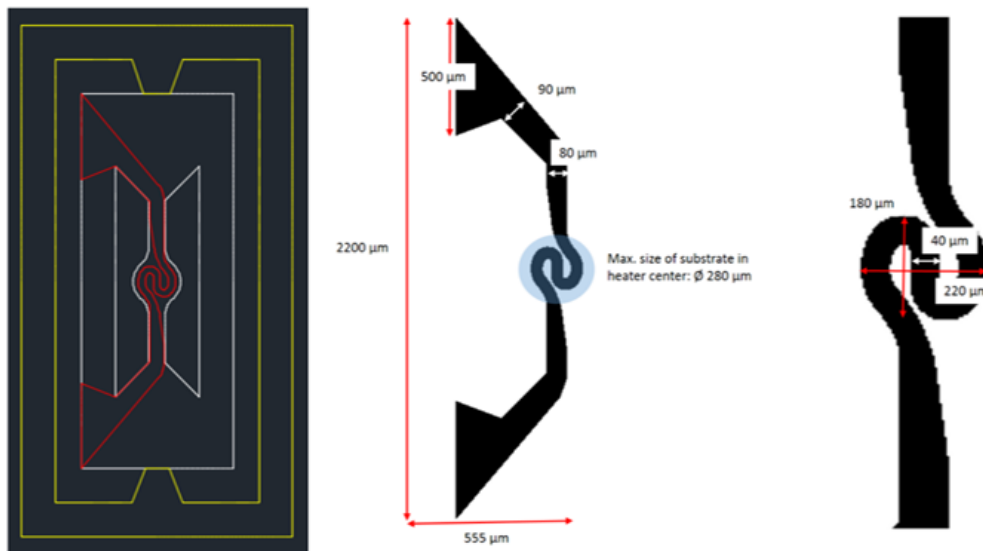


Figure 3: (left) Arrangement of the heater on the zirconia membrane and (right) miniaturized platinum heater layout.

**Table 2** summarizes the specifications of the printing layers and **Table 3** shows the target detection limits of the project gas sensor.

Table 2: Specification of the printed films for the gas sensor.

Ink film, function	Specification
Pt, heater	Heater resistance: 8-10 $\Omega \pm 20 \%$ Temperature range: 450 °C $\pm 10$ K (inner area of the hot zone) Power consumption: max. 500 mW @ 450 °C with 3 V power supply Cycling stability: $\pm 2 \%$ resistivity change after 1 million switch on-off cycles to 450 °C
Gas sensitive ink, sensor active layer	Sensitivity to methane, hydrogen, propane, CO gas
Ag- or Cu-inks, interconnect for packaging	3 to 20 times bulk resistivity

Table 3: Targets of gas detection limits of the gas sensor.

Toxic		Explosive	
Type	Detection limit (TLV)	Type	Detection limit (LEL)
CO	1 – 500 (25) ppm	CH <sub>4</sub>	0,1 – 2 (4,4 - 17) vol. %
NH <sub>3</sub>	1 – 200 (28) ppm	H <sub>2</sub>	0,1- 2 (4 - 96) vol. %
NO <sub>x</sub>	0,5– 10 (5) ppm	C <sub>3</sub> H <sub>8</sub>	0,1 - 1 (1,7 - 10,9) vol. %

#### 4.1.2 Temperature and humidity sensor layout and specification

**Figure 4** shows the principle layouts of the temperature and humidity sensor on mechanically flexible foil-based substrates. During the project various low-cost flexible substrates like polyethylene terephthalate (PET), polyethylene naphthalate (PEN) or paper were evaluated. For the project sensor demonstration, PET polymer foil (75  $\mu\text{m}$  thickness) was chosen for the temperature sensor and paper substrate (inkjet paper with 180  $\text{mg}/\text{m}^2$ ) was chosen for the humidity sensor.

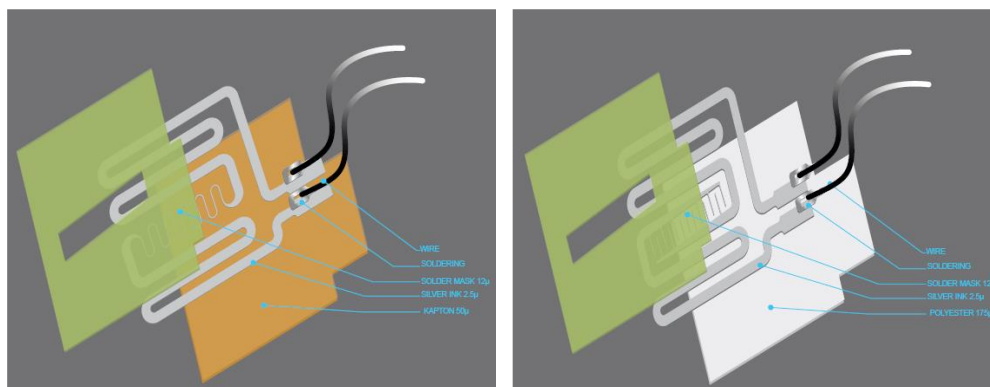


Figure 4: Principle layout of temperature (left) and humidity sensor (right).

**Table 4** summarizes the specification of the printing materials to fabricate the temperature and humidity sensors.

Table 4: Specification of the printed films for the temperature and humidity sensors.

Ink film	Specification
Ag, Cu	Film thickness: < 20µm Resistivity: < 30 µΩcm on average (~ 18 time Ag-bulk) Conductivity: > 3.3·10 <sup>6</sup> S/m on average Adhesion : best adhesion (ISO 2409) on all the substrates
Additional printing layers, materials	Dielectric ink (solder mask / hygroscopic material)

**Table 5** summarizes the target properties of the targeted project temperature and humidity sensors.

Table 5: Specification of the printed temperature and humidity sensors.

Sensor	Specification
Temperature sensor	Temperature range: 20 to 50 °C Sensitivity: ± 1 K Resistance: 100 Ohm and 1000 Ohm
Humidity sensor	Humidity range: 20 to 80 % Sensitivity: ± 10 %

### 4.1.3 Printed antenna

To connect several sensors in agricultural environments, a wireless sensor communication to transfer, collect and evaluate sensor information is needed. For the project, a low energy Bluetooth communication platform was developed (**Figure 5**), which operates at 2.45 GHz, is powered by a long-lasting lithium-battery (1.7 V – 3.6 V) and has a reading distance between sensor board and base station below 50 m (sufficient to connect a sensor network by using repeater). Additionally, a RFID tag was developed (Figure 6) to label the sensor device with individual sensor specific digital readable information (e.g. production lot, company information, application relevant information). This RFID tag allows a nearfield RFID NFC communication at 13.56 MHz and is fabricated by printing a 13.56 MHz coil with an integrated RFID chip.

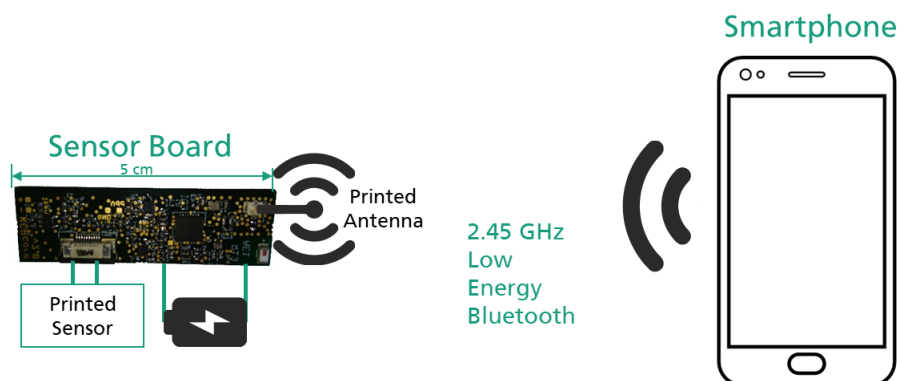


Figure 5: Low Energy Bluetooth sensor communication platform with chip “BLUENRG2” by ST (Fraunhofer ENAS).



Figure 6: Nearfield RFID NFC communication tag for digital sensor labeling.

## 4.2 Material developments

### 4.2.1 Silver and copper inks

Several ink formulations were developed, which were compatible to drop-on-demand inkjet printing or aerosol-jet printing. The inks printing compatibility was demonstrated with laboratory inkjet printers like Dimatix DMP-2800 series (10 pL print head) and Konica Minolta “KM 1024i” (6 to 30 pL) print head as well with an industrial print head from Ricoh “MH5421MF” (7 to 21 pL) for roll-to-roll production. As aerosol-jet printing equipment, the Optomec M3D system with 150 to 200  $\mu\text{m}$  nozzle size was used.

For the inks formulation and preparation, silver or copper particles were synthesized by developed wet chemical precipitation methods (**Figure 7**). To avoid nozzle clogging during the printing process, the maximum particle size was set to 200 nm.

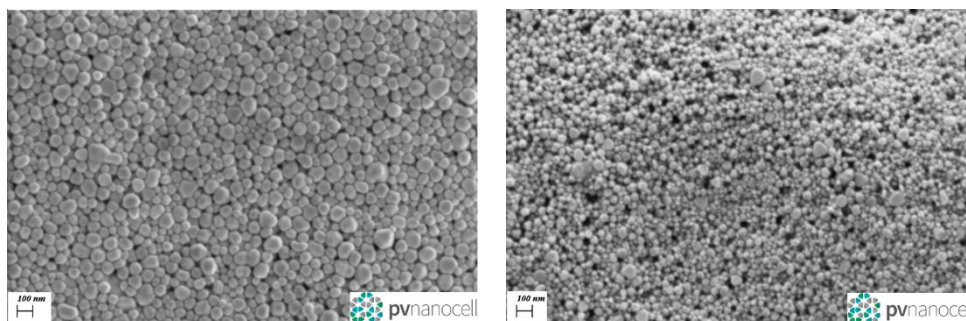


Figure 7: (left) Synthesized silver (mean particle size of 70nm) and (right) copper particles (mean particle size of 50 nm).

Based on the synthesized metal particles, several low viscous ink formulations were prepared and characterized. During the project different organic ink additives like dispersants and binders were evaluated. The influence of the metal solid content and type of solvents for the ink liquid carrier on the printed film quality was characterized. **Table 6** and **Table 8** summarizes the properties of the developed silver and copper inks, respectively.

Table 6: Properties of developed silver inks.

Silver inks	% Solids	Viscosity @25°C (cP)	Surface Tension (dyn/cm)	Additives
I40DM-106	40%	11	35	No additives
I50DM-106	50%	20	35	
I50TM-119	50%	39	30	Environmental reliability additives, withstanding humidity
I60PM-116	60%	38	23	

The silver inks were inkjet printed with test pattern on different polymer substrates like polyimide (e.g. Kapton), PET or even zirconia ceramic (Figure 8).



Figure 8: Silver ink "I50TM-119" on Kapton foil. (left) After printing and drying and (right) after sintering and 180 ° bending test.

The ink wetting behavior as well as achievable electrical conductivity and printed film adhesion was characterized (Table 7). The developed silver inks show even at low temperature annealing at 130 °C a low resistivity, which makes them suitable for printed electronics and sensors applications. The achieved silver films resistivity is only by a factor of 5 higher compared to silver bulk material.

Table 7: Properties of developed silver ink "I50TM-119" (\* contact angle by OWRK method, \*\* ISO 2409 Standard without cuts).

Substrate	Substrate Surface Energy *(mN/m)	Contact angle of ink	Sintering	Resistivity ( $\mu\Omega\text{cm}$ )	Adhesion **	Line width ( $\mu\text{m}$ )
Zirconia	50.2	8.9	240 °C/1hr	$8.8 \pm 0.9$	Pass	82
Kapton	44.8	12.1	240 °C/1hr	$9.0 \pm 0.5$	Pass	96
PET	39.7	32.4	130 °C/1hr	$8.7 \pm 2.4$	Pass	92

Comparable to the silver ink development, various copper inks were formulated and tested with variation of the metal solid content, type of solvent as well as variation of the copper particle size and synthesis parameters. Table 8 summarized different copper inks, which were further evaluated for printing compatibility.

Table 8: Properties of developed copper inks.

Copper ink	% Solids	Viscosity @25°C (cP)	Surface Tension (dyn/cm)
IC25EG-1	25%	32	45
IC40DM-7	40%	15	33
IC40DB-9	40%	16	29
IC50DM-7	50%	19	28
IC50TM-8	50%	30	25

The copper inks were inkjet printing on different polymer foils with variation of film width and thickness (Figure 9).

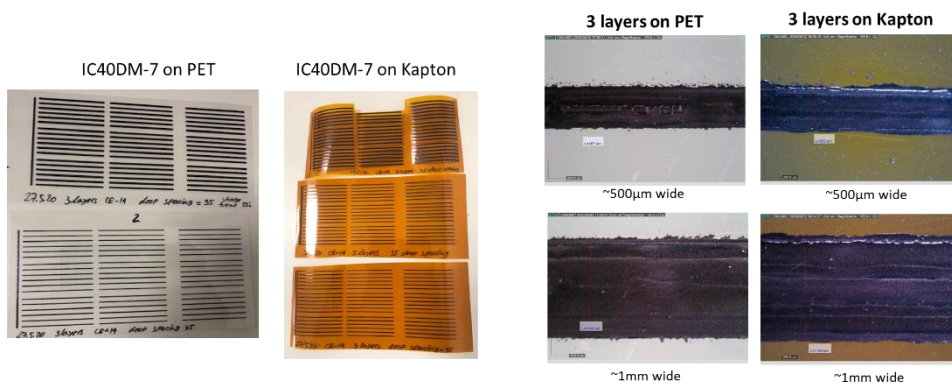


Figure 9: Printed copper ink "IC40DM-7" films on PET and Kapton polymer foils.

Based on these samples an optimization of the laser sintering procedure, which sinters the printed films within milliseconds with avoiding a total oxidation of the copper film even at air atmosphere, was done. A point laser (DPSS, 232 nm, Gaussian beam profile) as well as a 3 cm wide line laser (diode laser with 980 nm, Figure 26) was successfully evaluated for fast sintering of copper films (Figure 10). The copper film resistivities are only by a factor of 6 higher compared to bulk copper material.

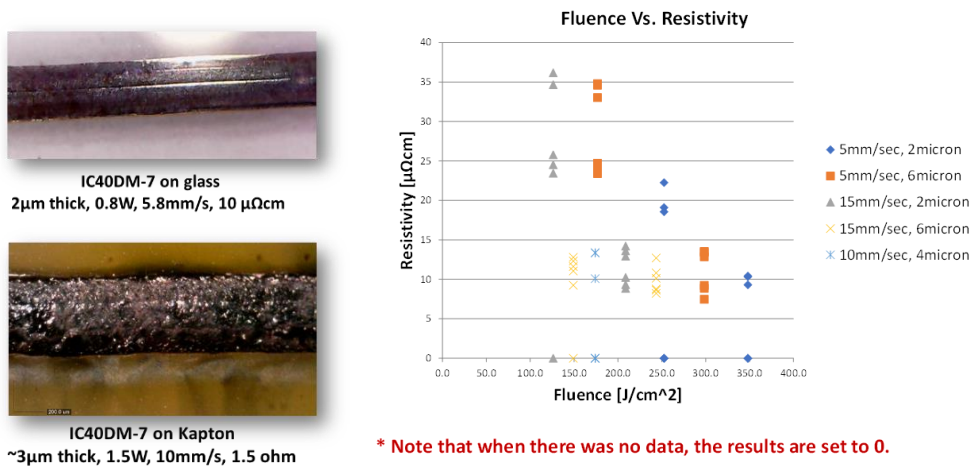


Figure 10: Laser sintering of inkjet printed copper films on PET and Kapton.

The developed ink synthesis routes were successfully scaled. The silver ink "I50TM-119" was scaled by a factor of 8, starting from 150 g batches at the project beginning to 1200 g for the preparation of the R2R printed sensor demonstrators. The copper ink "IC40DM-7" was scaled by a factor of 6, starting from 37 g at project start to 220 g batches.

#### 4.2.2 Platinum ink

Platinum particle inks, compatible to inkjet or aerosol-jet printing, were developed to achieve a printed heater, which can operate at elevated temperatures up to 500 °C, on a smooth zirconia substrate. **Figure 11** shows the strategy for the platinum ink development.

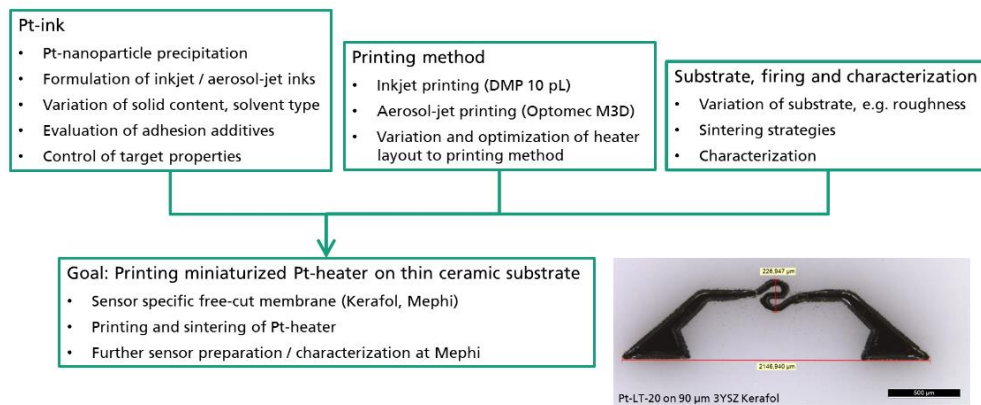


Figure 11: Strategy for the platinum ink development.

Comparable to the silver and copper ink development, the platinum ink synthesis started with a wet chemical precipitation of small platinum particles (**Figure 12**). This method was optimized during the project to achieve a high yield of the synthesized particles. Further, a recycling of not useable platinum raw material during the synthesis was established. This reduces the overall ink costs, if using expensive raw materials like precious metals.

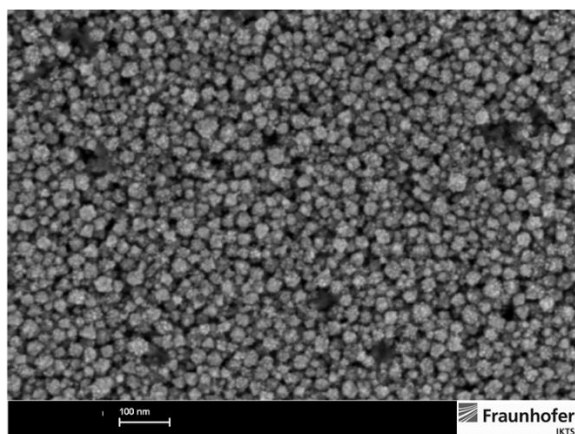


Figure 12: Synthesized platinum particles for the ink formulation (mean particle size of 50 nm).

Figure **13** shows the particle size distribution and the ink sedimentation behavior (example of a 20 wt.-% platinum ink). A maximum particle size of < 200 nm ensures a print compatibility with small inkjet nozzles, to avoid a nozzle clogging during the printing

process. The developed inks show a high sedimentation stability of only < 0.2 mm sedimentation of the particles per month, which leads to a high shelf life and ink usage above approx. 9 months.

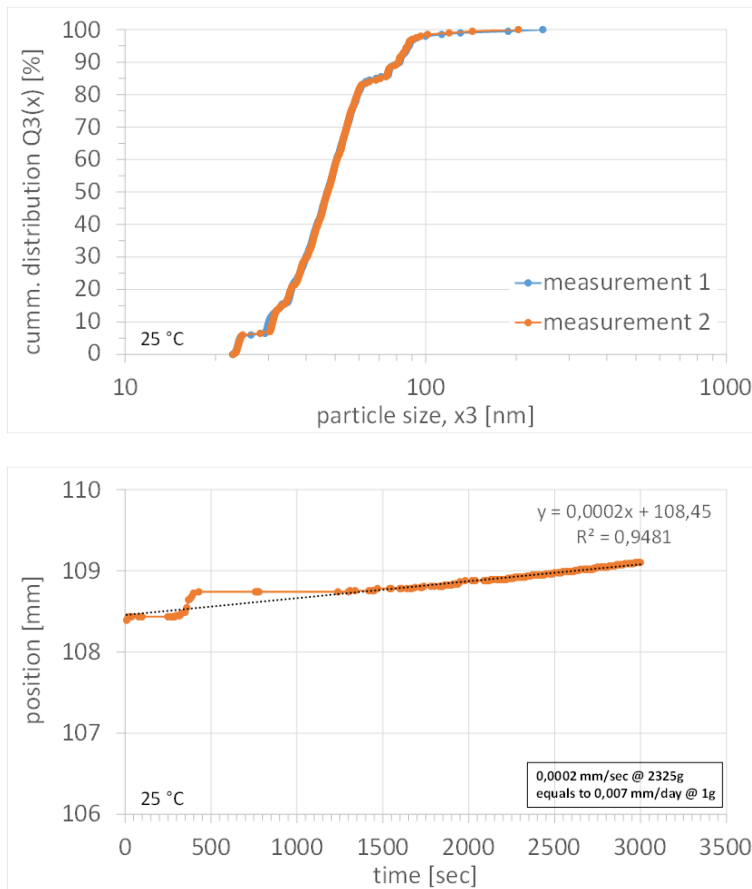


Figure 13: (top) Particle size distribution of a 20 wt.-% platinum ink and (bottom) sedimentation behavior of the ink in a centrifugal field (both measured by Lumiziser).

The platinum solid content in the inks was varied between 20 wt.-% to 40 wt.-%, which has an influence on the achievable print layer thickness in single pass printing. Different ink formulations were developed to achieve an ink viscosity and surface tension compatible to inkjet (8 - 11 mPas, 27 - 33 mNm) or aerosol-jet printing (2 - 6 mPas, 24 - 39 mNm).

The main issues for the platinum ink development were the achievement of an homogeneous ink layer together with a controlled ink wetting on an highly smooth zirconia substrate (roughness below 300 nm) and the sintered ink film adhesion on this substrate (**Figure 14**).

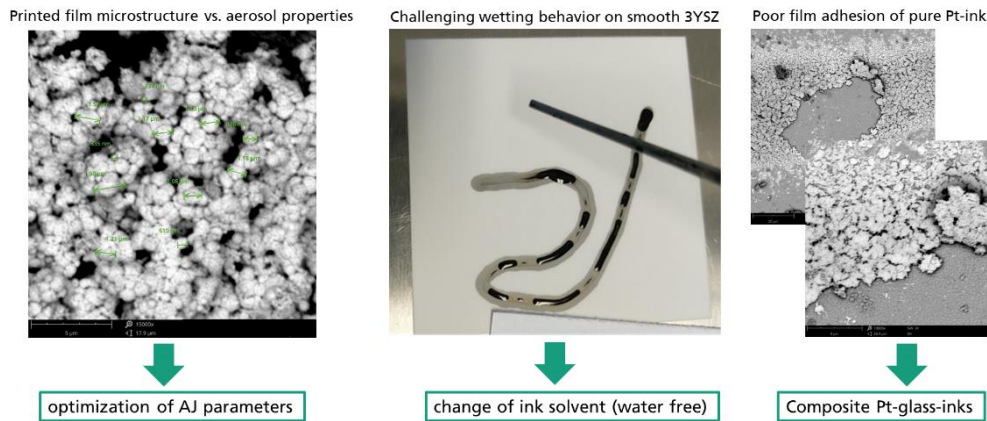


Figure 14: Main issues during the platinum ink development.

The principle wetting behavior of individual, larger Pt-ink droplets on the zirconia substrate was quite satisfactory (characterized by a drop shape analyser). However, during printing of larger amounts of ink, an unusual dewetting of the ink film was observed (Figure 14). Thereby the ink seems first to wet the substrate, but pulls together in itself shortly after. By changing the ink liquid carrier from water based to water-free alternatives, a better homogenization of the printed and dried film was achieved (Figure 15).

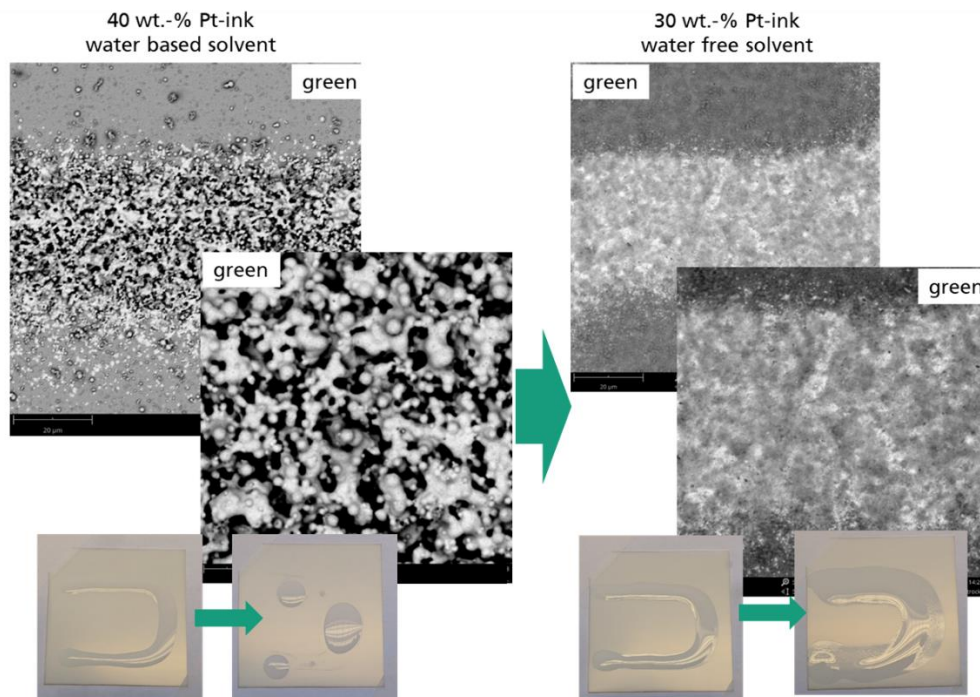


Figure 15: Comparison of aerosol-jet printed and dried Pt-films on zirconia substrate based on (left) water based ink solvent and (right) water-free ink solvent (bottom pictures show the wetting of the ink solvent carrier).

Further, the control of the aerosol-jet printing parameters was found to be a crucial point to achieve more homogeneous film microstructures.

To achieve a film adhesion on ceramic substrates, usually glass powders are used in thick film pastes. Such powders are not directly useable for inkjet or aerosol-jet inks, since their particle size is too large, which leads to fast sedimentation (due to very low ink viscosity)

and nozzle clogging. By applying an intensive milling procedure of suitable glass powders in ceramic grinding media, it was possible to reduce to glass particle size below 200 nm (**Figure 16**). The observed increased platinum film adhesion after sintering was due to a softening of the glass powder in the printed film, which wets the ceramic surface and leads to the formation of adhesion points between platinum metal and zirconia.

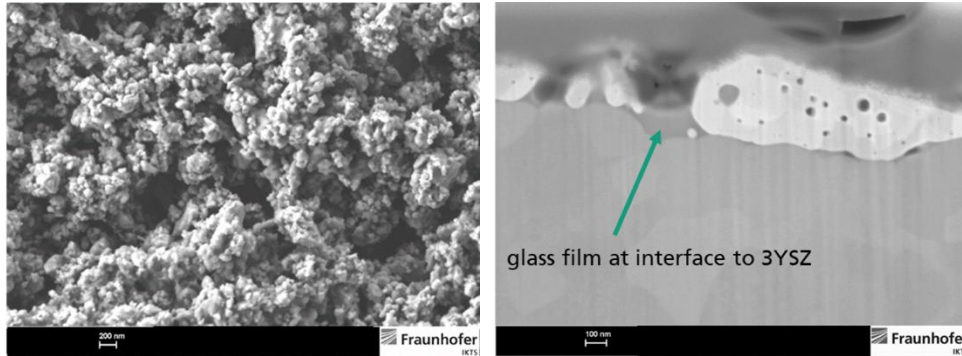


Figure 16: (left) Glass powder after intensive high-energy milling procedure with particle size below 200 nm and (right) cross section of a sintered Pt-glass-composite-ink on zirconia with formation of a glass adhesion layer.

### 4.2.3 Gas sensitive materials

For the gas sensitive electrode of the MOX gas sensor several nano-powders were synthesized (Table 9) and dispersed in proper solvents to form a printable ink suspension (drop coating).

Table 9: MOx ink materials for gas sensing.

Gas species	Metal oxide material
O <sub>2</sub> , NO <sub>2</sub>	WO <sub>3</sub>
NO <sub>2</sub>	ZnO
H <sub>2</sub>	SnO <sub>2</sub>
NH <sub>3</sub>	SnO <sub>2</sub> (Pd)
CH <sub>4</sub>	SnO <sub>2</sub> (2Pd:1Pt)
CO	SnO <sub>2</sub> (3Pd:1Pt)

### 4.2.4 Thin zirconia substrate

An ultra-thin zirconia membrane for the „low power“ gas sensor was developed. During the project it was possible to decrease the substrate thickness, starting from 90 µm at the project beginning, to only 20 to 40 µm. This reduces the overall substrate mass of the sensor membrane, where the on top printed heater will only need a very limited amount of power to run during operation (< 100 mW feasible).

For the development of such thin ceramic substrates, the material zirconia (3YSZ) was chosen, which combines high fracture toughness, flexural strength, high chemical and temperature resistance with processability.

Several 3YSZ raw material powders were evaluated in a typical ceramic processing route of slurry preparation, tape casting of thin foils and sintering (**Figure 17**).

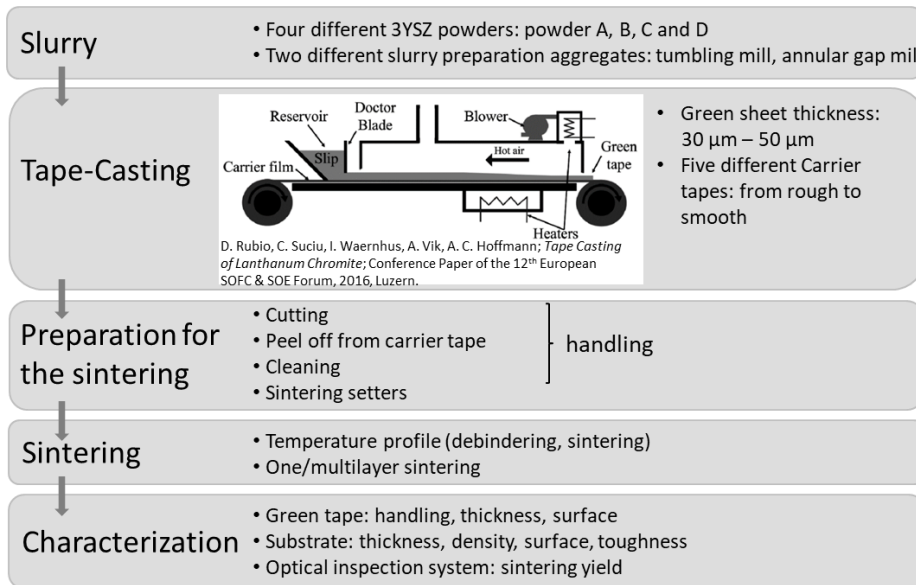


Figure 17: Workflow for zirconia substrate development.

The fabricated green tapes were cut into smaller sizes for debinding and sintering experiments. After sintering the final substrate samples were cut by laser. Table 10 summarizes the ceramic substrate processing steps and parameters.

Table 10: Ceramic substrate processing parameters.

Parameter	value
Green tape processing	Batch sizes of 0.3 - 1 m width and 10 - 150 m length
Green tape thickness	30 to 80 $\mu\text{m}$
Debinding	200 to 600 $^{\circ}\text{C}$
Sintering	$\sim$ 1400 $^{\circ}\text{C}$
Substrate size	5 x 5 $\text{mm}^2$ to 50 x 50 $\text{mm}^2$

During the project, due to improvements in surface quality, yield and low surface roughness after sintering, mechanically stable and even bendable substrates were demonstrated (Figure 18).

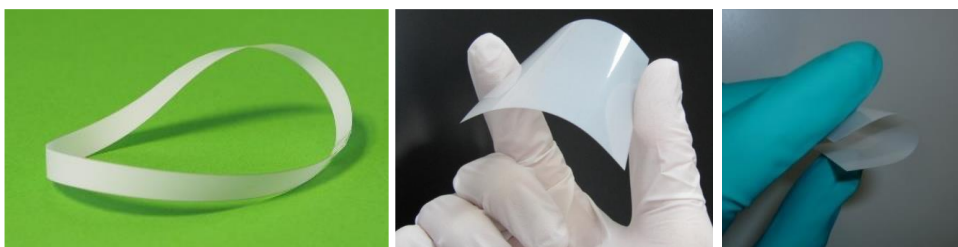


Figure 18: Zirconia (3YSZ) substrates with 40  $\mu\text{m}$  (left, middle) and 30  $\mu\text{m}$  thickness (right).

**Table 11** summarizes the properties of the developed zirconia substrate, which was used as a ceramic membrane for the project MOX gas sensor.

Table 11: Zirconia substrate material.

Parameter	value
Material	3YSZ
Substrate size	50 x 50 mm <sup>2</sup>
Thickness	< 40 μm
Roughness top / down side	R <sub>a,top</sub> < 0,4 μm, R <sub>a,down</sub> < 0,3 μm
Density, porosity	ρ ≥ 6 g/cm <sup>3</sup> , porosity < 1 vol.-%
Flatness, curvature	20 μm @ 50 x 50 mm <sup>2</sup>
Temperature stability	1000 °C

An optical inspection system for the detection of surface defects after substrate sintering was established (**Figure 19**). With this equipment a fast and reliable detection of even small defects like particle agglomerates can be detected in high resolution and throughput for quality control.

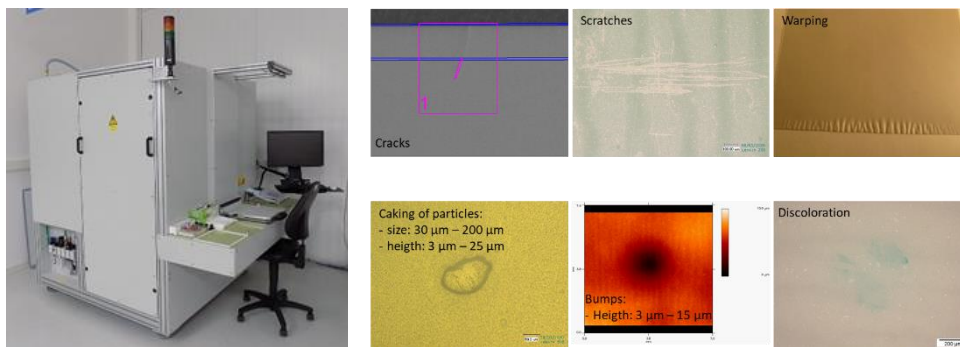


Figure 19: (left) optical inspection system and (right) examples of defect classification.

The achievable yield of high-quality substrates without defects depends mainly on the processability of the raw ceramic powder and on the final substrate size. Yields above 60 % were achieved for laser cut substrate sizes of 30 x 30 mm<sup>2</sup>. An economic estimation of the production costs of a 40 μm thin substrate with 100 x 100 mm<sup>2</sup> size, leads to a price indication of 20 Euro, if 10.000 pcs/month are produced.

### 4.3 Gas sensor with ceramic membrane and package

For the development of the MOX gas sensor, several fabrication steps were evaluated. The thin zirconia membrane was mechanically laser milled (“micro-milling”), to realize a free cut sensor chip according to **Figure 2**. This sensor chip has a low thermal mass, which leads to a low power consumption of the sensor heater during operation. On one side of this membrane a miniaturized platinum heater was printed. On the opposite side, platinum connections were printed as well as a gas sensitive ink to realize the gas sensing electrode. This sensor chip is placed in a customized ceramic housing, consistent of a top and bottom part. For this housing, thicker alumina ceramic substrates were processed with micro-milling to realize 3D-shaped housing parts, which were glued together. This package, in a SOT-23 form factor, can be connected by soldering to well-known package standards like TO-8 package, which are used for gas sensing tests.

### 4.3.1 Printing of platinum heater and sensing electrode

The developed platinum ink was first tested by using a laboratory inkjet printing system from Fujifilm Dimatix (**Figure 20**).



Figure 20: Fujifilm Dimatix inkjet printer DMP-2831 with 10 pl print head.

The target print layout (**Figure 3**) was evaluated by printing several bitmaps with variation in dpi (drop space) and film thickness (number of print layers). The results showed that the outer contour size of  $\sim 0.5 \times 2 \text{ mm}^2$  of the desired heater layout is achievable by inkjet printing. However, the inner core part of the heater, a miniaturized meander of  $40 \mu\text{m}$  line width on a max. area of  $200 \mu\text{m}$  in diameter, was not possible with inkjet printing. Due to a too high drop volume and ink wetting on the smooth zirconia substrate, the minimum drop size after printing was determined to be  $80 \mu\text{m}$  (**Figure 21**).

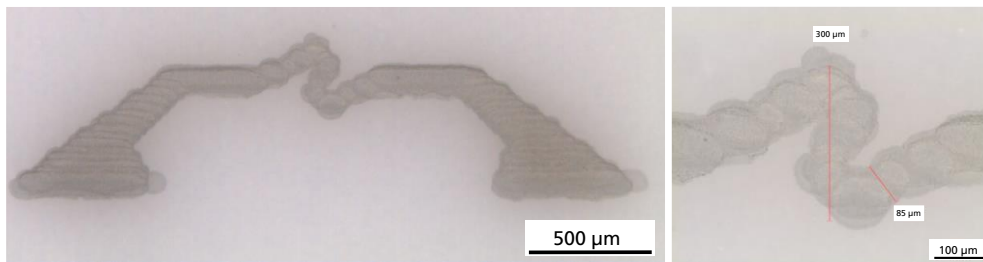


Figure 21: Inkjet printed platinum heater on zirconia substrate.

Therefore, an alternative printing method, the aerosol-jet printing with an ultrasonic ink atomization, was used (**Figure 22**). During the aerosol-jet printing, the platinum ink is atomized in small droplets, which are collected in an aerosol-stream and sprayed on the substrate.

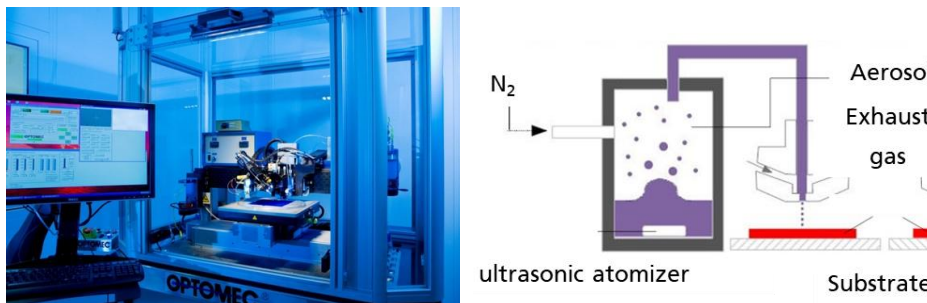


Figure 22: Aerosol-jet printer M3D from Optomec, USA.

With control of the aerosol parameters, the printing of the target platinum heater with small line widths of approx.  $40$  to  $50 \mu\text{m}$  was possible (**Figure 23**).

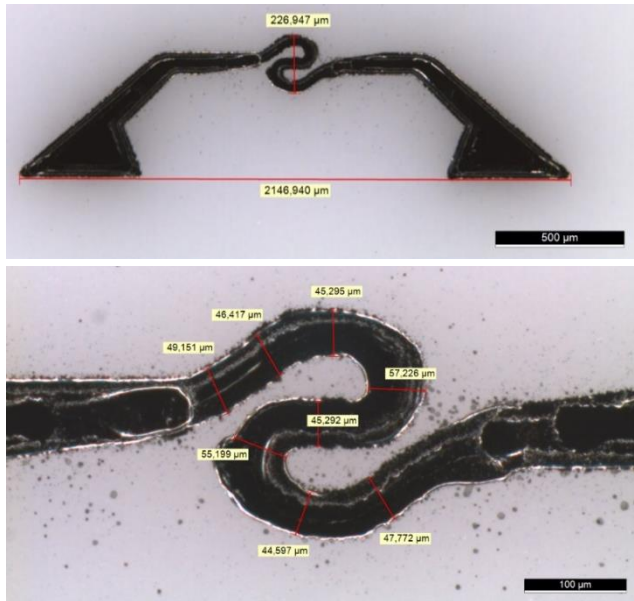


Figure 23: Aerosol-jet printed platinum heater on zirconia after drying.

The platinum film thickness in the range of 1 to 5  $\mu\text{m}$  could be adjusted by the variation of the print layer numbers (3 to 10 times printing). **Figure 24** shows two printed miniaturized platinum heaters, with optimized printing parameters for the developed Pt-glass-ink, before and after the furnace sintering.

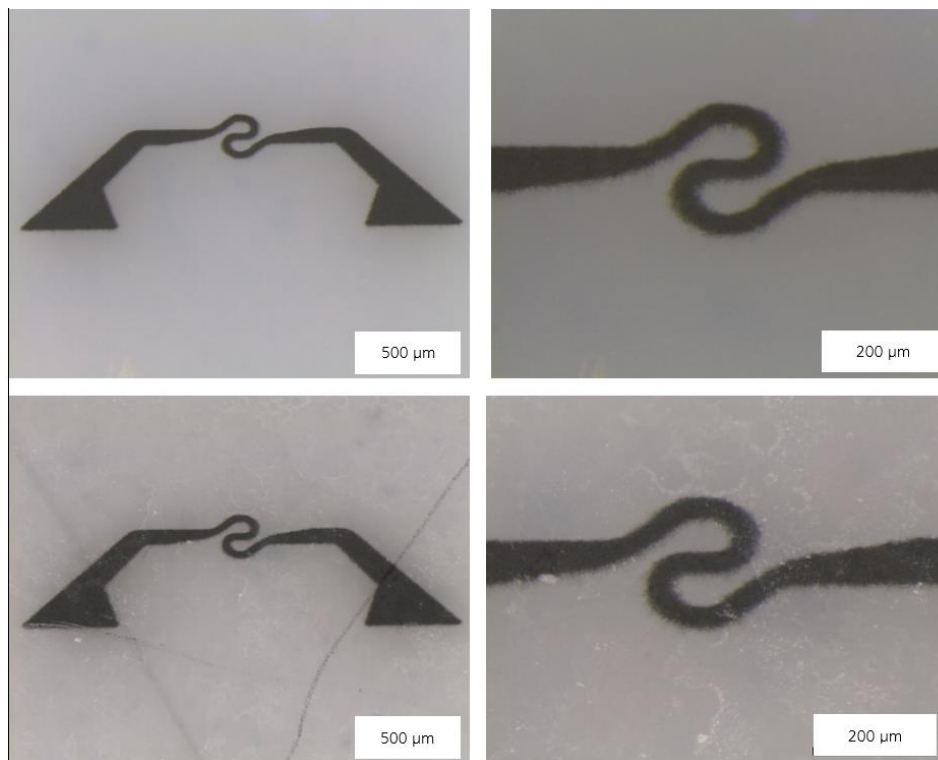


Figure 24: (top) Printed heater based on Pt-glass-ink after drying at 80 °C and (bottom) heater after sintering at 760 °C in a muffle furnace.

After sintering the resistance of the heater was in the desired range of 16 to 40 Ohm, which works well with the sensor driving electronics.

The microstructural characterization of a pure platinum ink film revealed, that with conventional sintering in a muffle furnace, a pronounced grain coarsening and “island” formation of the platinum film occurs. This effect is even more pronounced with increasing sintering temperatures (**Figure 25**). Even with the developed water free platinum inks, some inhomogeneity of the printed green film remained, which seems to prevent the forming of a homogenous and dense platinum film during sintering.

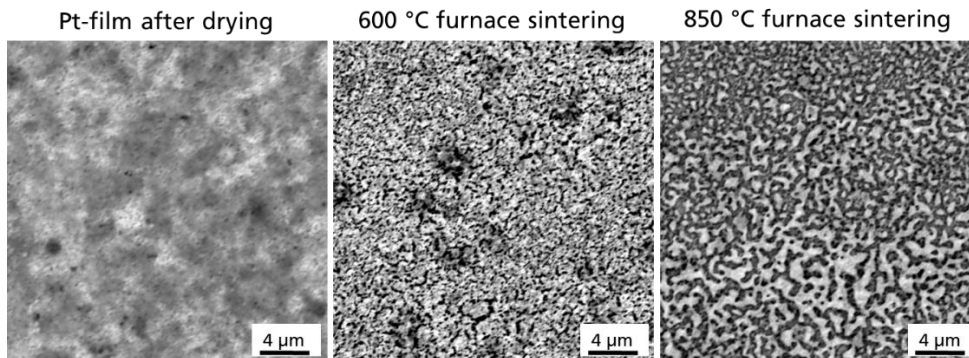


Figure 25: SEM analysis of printed platinum films after drying and sintering in a furnace.

As an alternative to traditional furnace sintering a line laser, with processing times within milliseconds, was evaluated to sinter the printed platinum films. The IR laser with 980 nm uses a diode laser array with continuous wave operation and a micro-optical optimization of the light beam (“top hat” profile) to generate a laser spot in shape of a line of 30 mm x 0,1 mm size. The sample is transferred with defined speed under this laser beam and the sintering of the printed metal films takes place within milliseconds (**Figure 26**).



Figure 26: High-power diode laser sintering (HPDL) of printed films.

By using this HPDL process, well conductive Pt-heater of approx. 30 Ohm resistance were realized (**Table 12**).

Table 12: HPDL laser sintering of printed heater with Pt-glass-inks.

Platinum ink	Velocity, mm/min	dwell time, ms	Intensity, kW/cm <sup>2</sup>	Fluence, J/cm <sup>2</sup>	R <sub>heater</sub> , Ohm
Glass-power I, water-based	500	12	6,8	82,0	30
Glass-powder II, without water	700	8,6	10,9	93,7	93

The microstructural analysis of the laser sintered platinum heaters, based on a platinum-glass-ink, revealed that the film is not complete homogenous and dense (**Figure 27**). The platinum grains show a particle sintering (sinter neck formation). The particle size of approx. 100 to 200 nm remains rather small, which means that the laser sintering is so fast, that an extended particle coarsening is avoided. It seems, that the film inhomogeneities were already present in the dried film after printing, which means that further developments are needed to improve the platinum ink as well as the film quality during printing.

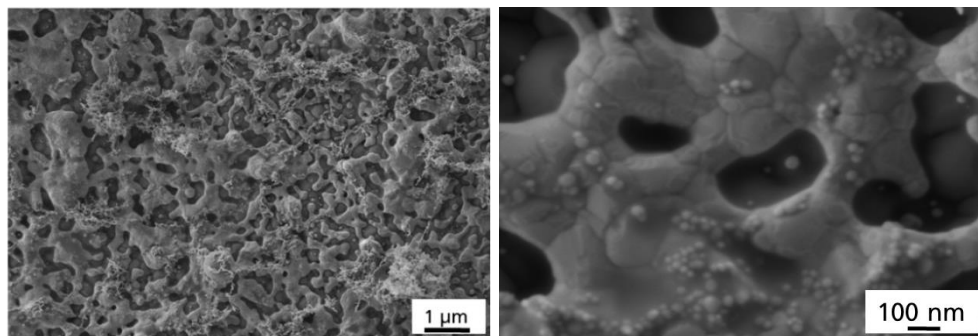


Figure 27: SEM analysis of the surface microstructure of a HPDL sintered platinum-glass film on zirconia.

An X-ray-fluorescence (XRF) analysis revealed that the printed platinum mass on the zirconia substrate varied a lot during the printing process (**Figure 28**). There is a clear correlation between the mass of printed platinum ink and the achievable resistance of the heater after laser sintering. The variation in platinum mass per unit area (core part of heater meander) is attributed to the printing process, where the ink is not atomized homogeneously and tends to vary with printing time.

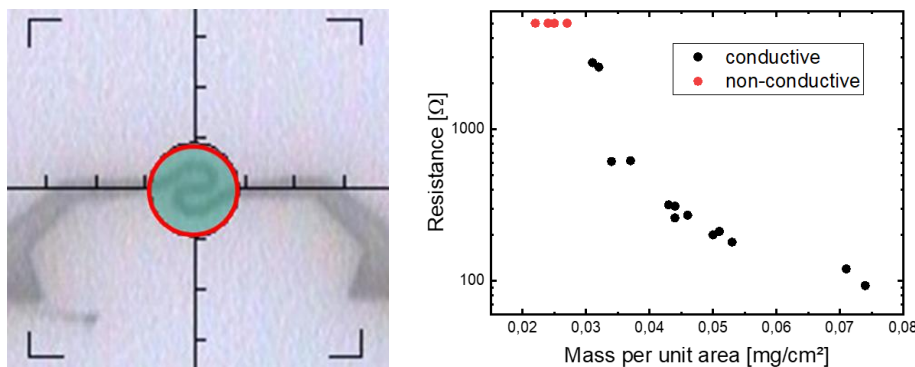


Figure 28: (left) XRF analysis of printed platinum heaters with (right) correlation of the platinum mass per unit area to the heater resistance after laser sintering.

The functionality of the sintered Pt-heaters was demonstrated by using an IR camera setup (**Figure 29**). Therefore, individual heater chips of 3 x 5 mm<sup>2</sup> size on 90 μm thick zirconia substrate were cut by laser and contacted with a platinum paste to platinum wires.

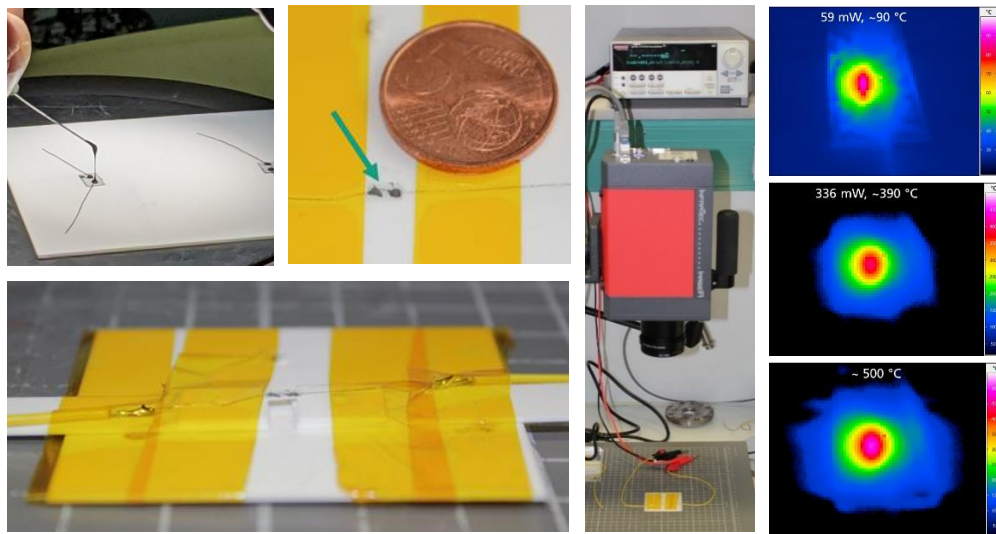


Figure 29: Set-up for platinum heater test (printed on 90 μm thick zirconia) with contacting and IR camera equipment.

For the heater test, a small heater chip is placed “hollow”, like a bridge, between two ceramic substrates, to simulate the latter case of a free-cut membrane in the MOX gas sensor setup. By controlling the current (starting with low mA), the measurement of the heater surface temperature by IR camera and the voltage it was possible to calculate the heater power consumption. The results demonstrate that a heating of up to 500 °C is possible with such a miniaturized printed platinum heater. For these tests a rather thick zirconia substrate (90 μm) was used as a standard thickness for the general printing development. That is why the power consumption of the heater of approx. 400 mW was rather high. To illustrate the potential of the project idea of a “low-power heater”, a shadow mask magnetron sputtered platinum heater on only 50 μm zirconia was characterized and showed < 150 mW at 500 °C working temperature (**Figure 30**). The lowest power consumption was demonstrated by using a 20 μm zirconia substrate with only 95 mW power consumption at 500 °C.

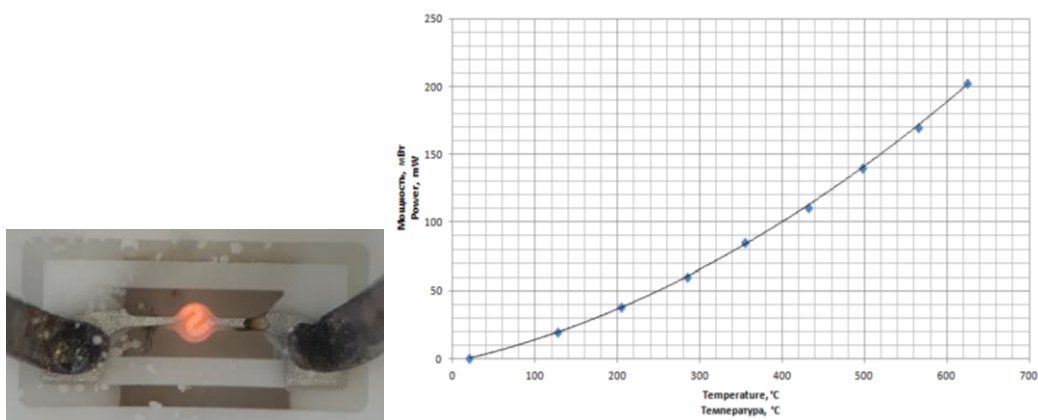


Figure 30: (left) Sputtered Pt-heater on 50 μm zirconia membrane (free-cut hot-plate of 280 μm size) and (right) power consumption tests.

### 4.3.2 Fabrication of ceramic package and sensor assembly

The developed thin zirconia membrane was mechanically cut by a laser micro-milling technology. With this technique, free-cut sensor chips with a small hot-plate (size of 280  $\mu\text{m}$  in diameter) were fabricated out of 30  $\mu\text{m}$  thin zirconia substrates. **Figure 31** and **Figure 34** show, that this approach is scalable to fabricate arrays of several individual sensors.

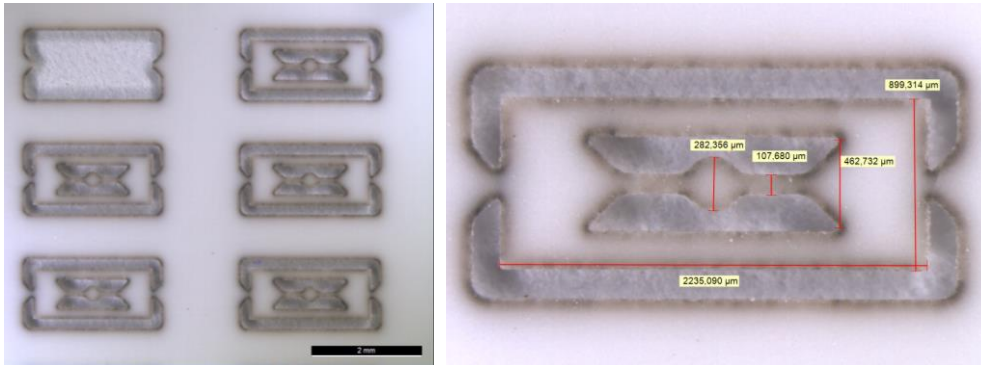


Figure 31: Array of sensor chips of 30  $\mu\text{m}$  thin zirconia prepared by laser micro-milling.

In the project a special tool was developed, which combines the digital software planning in 3D with the laser micro-milling and the direct printing of MOX gas sensitive materials of the gas sensing electrode (**Figure 32**). All parts of gas sensor were fabricated by a totally digital technological flow by using a pre-developed 3D model in STL format, which is customary in a rapid prototyping way.

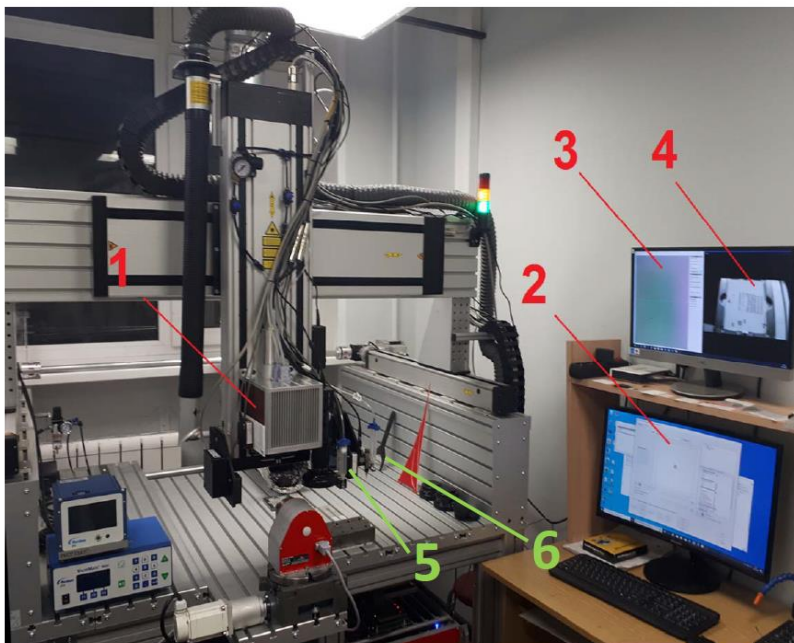


Figure 32: Integration of an ink-jet printing tool with a laser micro-milling system: (1) laser scanner with integrated hardware; (2) graphical interface of the implemented 4-coordinate laser micro-processing control software; (3) displayed image of milled area from a microscope with amplifying up to 2000 times; (4) constantly displayed camera image to monitor the processing area; (5) XQR41 Series Traditional Pneumatic Valve kit with 150  $\mu\text{m}$  dot diameter ; (6) PICO jet valve set with 50 micron nozzle.

The outer MOX gas sensor package was made of 96 %  $\text{Al}_2\text{O}_3$  material with 1000  $\mu\text{m}$  (bottom of package) and 500  $\mu\text{m}$  (top cap) thickness, which is cut in 3D shape of a SOT-23 package (**Figure 33**). This package consists of two half components. In between the top and bottom part of this package, the thin zirconia sensor chip is placed and contacted by silver ink printing.

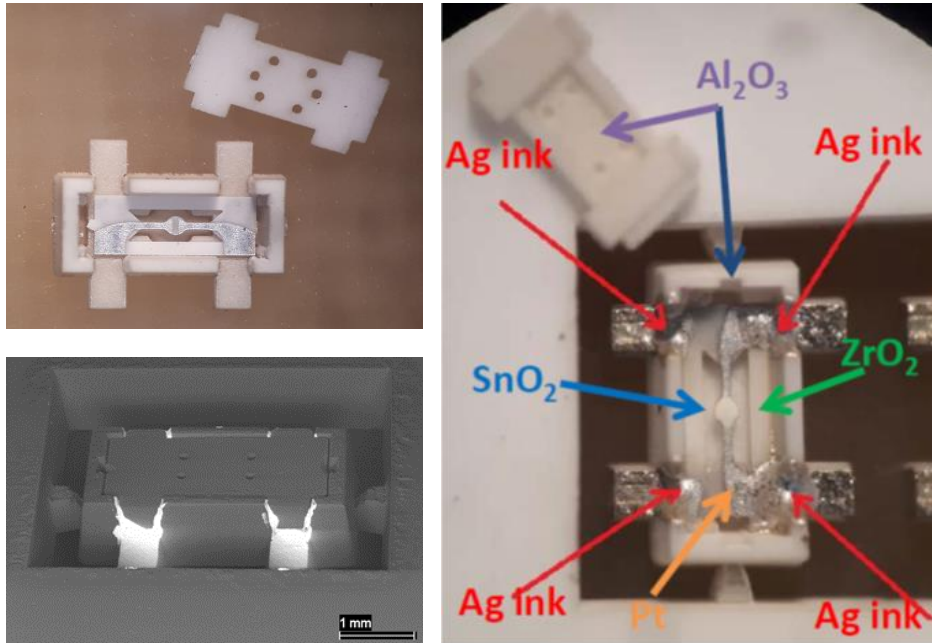


Figure 33: Ceramic MOX gas sensor housing in a SOT-23 package form-factor with dimension  $1.4 \times 3.0 \times 1.00$  mm.

Due to the possibility of the parallel processing of a lot of individual small MOX sensor components, which are arranged as an array on a larger ceramic substrate, the developed micro-milling technology is a very powerful tool to realize such miniaturized ceramic MOX sensor components economically. **Figure 34** illustrates the fabrication of 306 sensor package out of only 3 ceramic substrates of  $48 \times 60$  mm<sup>2</sup> size. The high packing density of the sensor components on one single alumina substrate was only possible due to the high quality of the developed ceramics, which possess a high mechanical strength during the laser ablation process.

**306 samples of SOT-23 packages on 3 substrates**

17x9=153 for 1x60x48 and  
35x9=315 for 0.5x60x48 Al<sub>2</sub>O<sub>3</sub> substrates

5x10=50 for 0.04x30x48  
ZrO<sub>2</sub> membrane

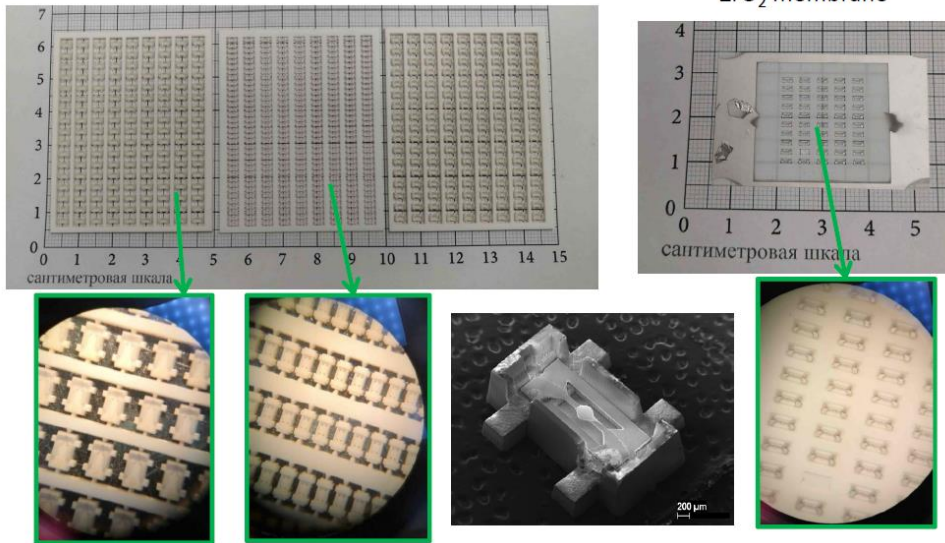


Figure 34: Scaling of micro-milling fabrication of MOX sensor packages and zirconia hot-plates.

Another important property of the ceramic materials used for the gas sensor package is their compatibility with standard soldering processes for microelectronic products on PCB using ENIG coating. During first tests a "floating" (**Figure 35**) of the sensor package in the tin-based solder was observed. For testing a range of fluxes and solders variety, a PCB with an immersion gold-plated layer was manufactured. It was found that the soldering of the silver ink metallization is possible by using a flux based on ALPHA® 615 Super RMA material.

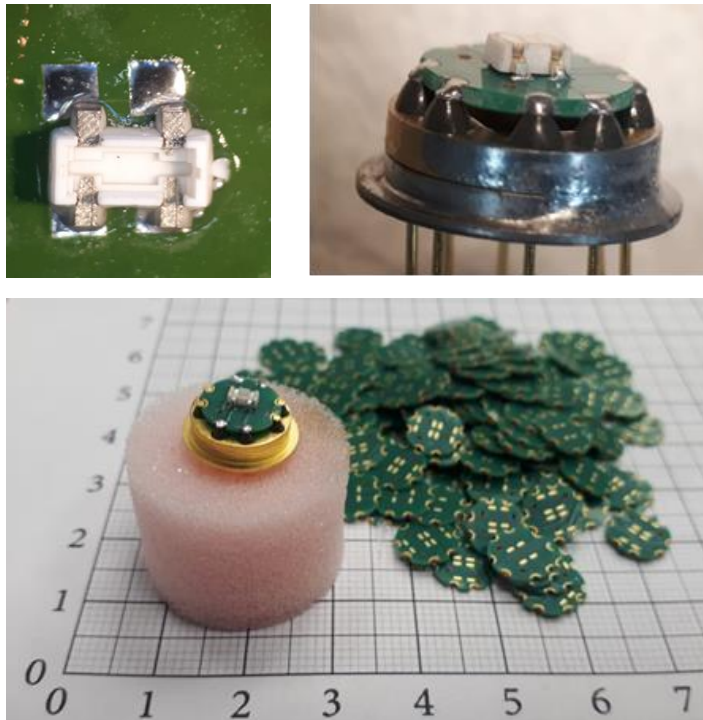


Figure 35: (top left) Floating effect of a sensor package with silver ink metallization in a soldering paste; (top right) soldered sensor package with flux; (bottom) gas sensor assembled in TO-8 package by using a standard PCB with ENIG coating.

### 4.3.3 Gas sensor testing

For the electrical contacting of SMD miniaturized sensors, usually a soldering or the use of special adapters, like DIP6-SOT23-6, is necessary. Often the sealing creates problems during testing. In the project the developed MOX gas sensors were soldered onto a TO-8 package, which contains a steel mesh and is certified for explosion protection. This makes the overall handling of the sensors easier, because the form-factor SOT-23 is the smallest, which is used for MOX gas sensors nowadays. The TO-8 based assembling is placed in a sealed chamber, where various gases can be applied for testing. Alternatively, the sensor was capped with a small cylinder, where various gases can flow through (**Figure 36**).

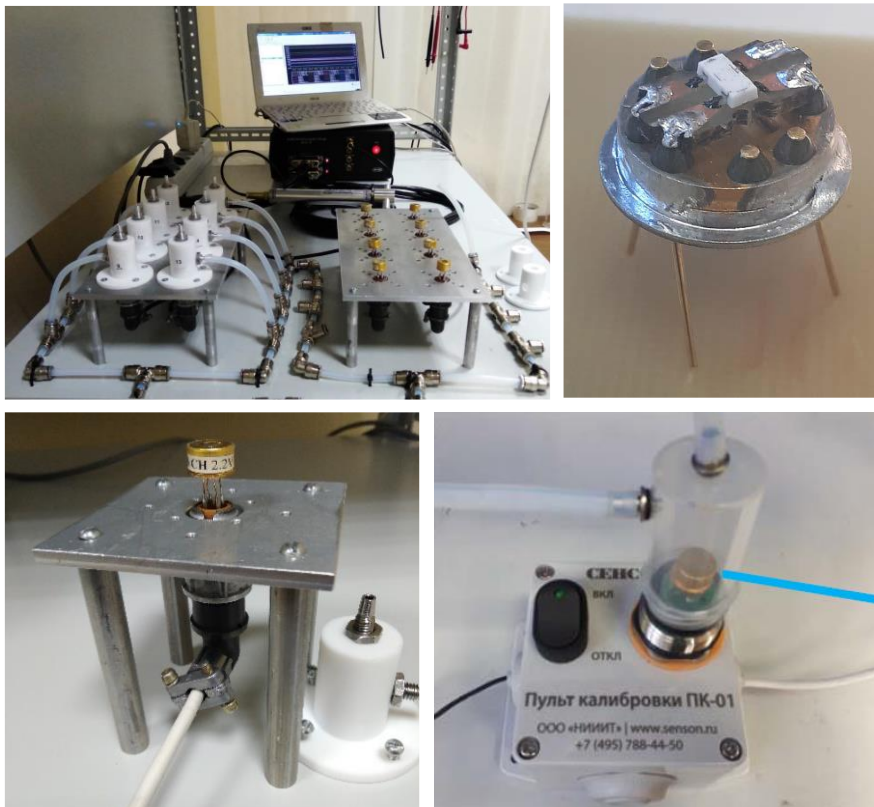


Figure 36: Gas sensor testing equipment (Mephi and RIIT).

**Table 13** summarizes parameters of the developed gas sensor demonstrator. The gas sensor (Figure 37) was finally assembled by the company RIIT. The demonstrator illustrates the use in agricultural applications. It is based on a PWM module, which includes an impulse heating of the MOX semiconductor sensor.

**Table 13:** Parameters of developed gas sensor demonstrator.

Parameter	Range of settings
Dimensions	25 × 25 × 35 mm
Weight	no more than 30 g
Explosion protection level	1Ex ia d IIC T4 Gb X
protection of the case against external influences	not less than IP65
Sensor types	Optical, semiconductor, thermocatalytic, electrochemical
Average service life	10 years
Output signals:	digital serial channel UART
Pressure	84 to 120 kPa
Relative humidity	Up to 95%, non-condensing
Ambient temperature	-60 ... + 50 ° C
Power consumption	1 W
Supply voltage:	3.15 ± 0.05 V



Figure 37: MOX gas sensor demonstrator (RIIT).

Before the gas test, the sensors were pre-aged in air at a constant working mode at 450 °C (**Figure 38**). This procedure is necessary to stabilize the sensor signal (especially the gas sensitive MOX sensing layer response) as well as to prevent possible failures of the microhotplate due to silver particle electromigration from contact pads on the ceramic package. After this pre-aging step, the resistance of the sensor microhotplate was stable at a level of 8 to 10 Ohm at 20 °C and the sensors were ready for gas sensitivity tests to important agricultural gases like NH<sub>3</sub>, CH<sub>4</sub>, NO<sub>2</sub> and H<sub>2</sub>. This stability of the platinum microhotplate resistance is key for a long-term working mode in real applications.

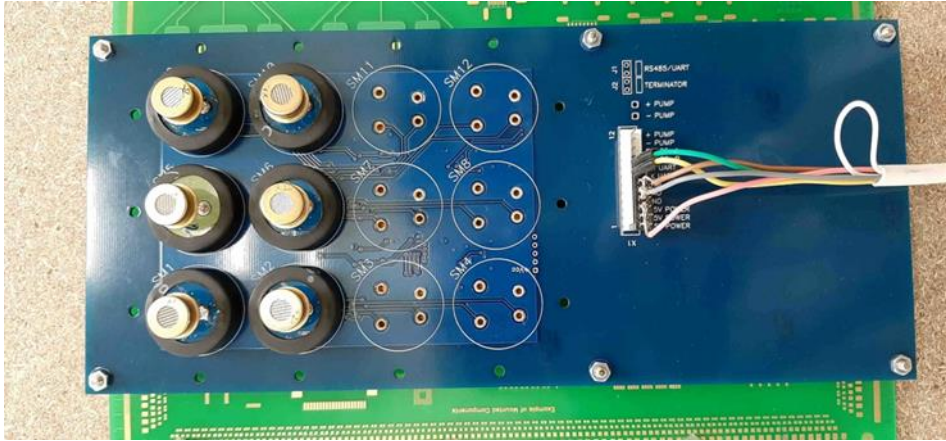


Figure 38: Pre-aging of MOX gas sensors on a demonstrator electronic module (RIIT).

The tin oxide based gas sensitive layers show in air a resistance range of 100 MOhm to 10kOhm. A typical dependence of this resistance from the supply voltage is shown in **Figure 39**. With increasing supply voltage, the temperature of the hot plate rises. On average, with a 1.5 supply voltage the necessary 430 °C working temperature is reached (temperature coefficient of resistance for micro heater is 0,0025 1/K). Tin-based gas-sensitive materials (tin oxide plus Pt and/or Pd catalysis) are in a stationary mode, if heated to 450 °C. At this temperature, no difference in sensitivity was observed for various gases in low concentration.

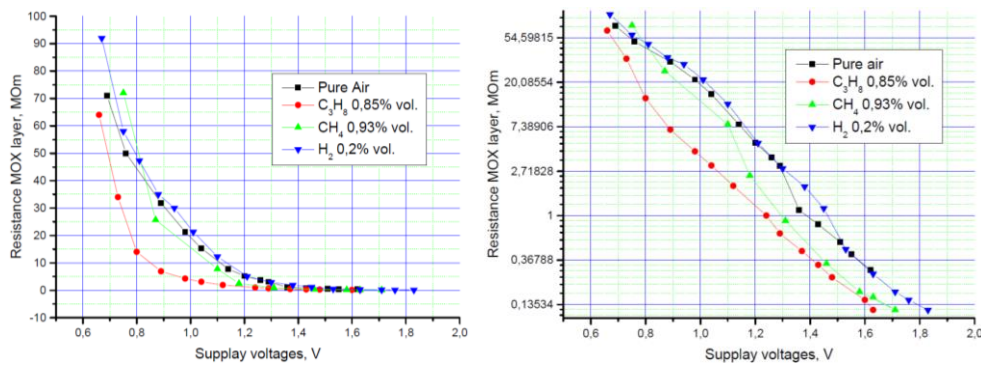


Figure 39: Dependence of the sensor signal resistance from the supply voltage.

The strategy for gas testing was based on the choice of gas sensing materials with the highest sensitivity to micro concentrations of toxic substances - first of all, ammonia. Ammonia is a widespread chemical, which is often used, forms in agricultural environments and which amount must be carefully controlled (e.g. fertilizer). It was found that the self-developed MOX gas sensitive material (tin oxide doped with palladium) showed the highest sensitivity to ammonia among other testing gases. Fabricated gas sensors with this sensing material were successfully tested in a temperature pulse mode, where the heater increases the hot-plate temperature between 110 °C to 450 °C for a short time. The gas sensing takes place during the first second of heating of the sensing material (**Figure 40**). A second set of tests was performed for high concentrations of flammable gases such as hydrogen and methane. In the presence of nitrogen dioxide, a reduced conductivity of the sensing electrode compared to pure air was observed.

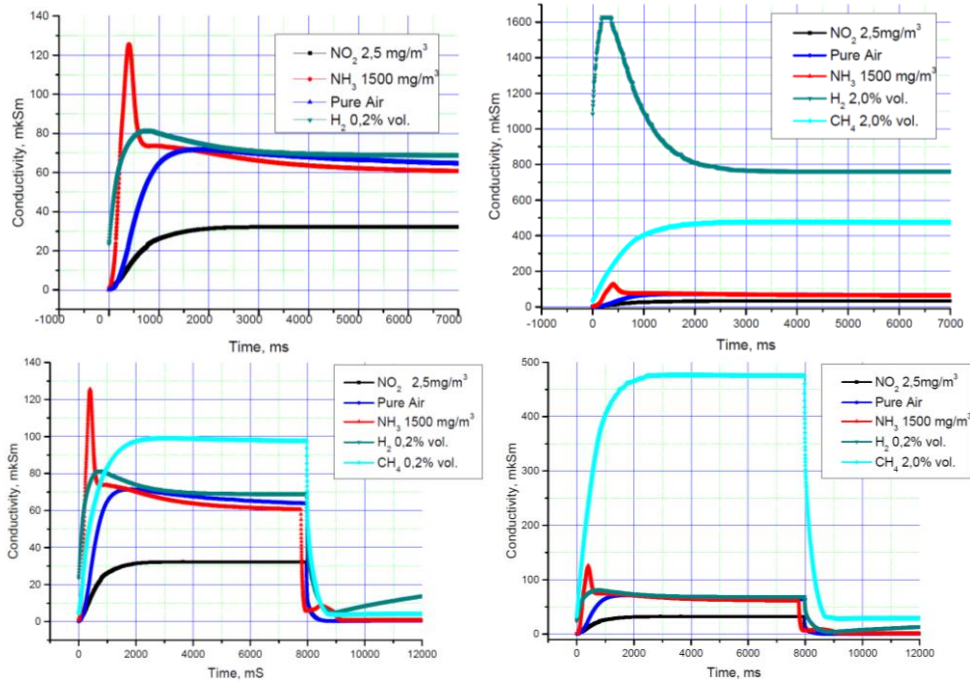


Figure 40: Gas sensing test of the developed MOX gas sensor.

The developed sensors showed no visible response to low concentrations of flammable gases like 0.2% vol.  $\text{CH}_4$  or 0.2 vol.-%  $\text{H}_2$ . But for dangerous concentrations for human staff in agriculture relevant environments the sensors showed a visible response to 1500 mg/m<sup>3</sup>  $\text{NH}_3$ , 2.5 mg/m<sup>3</sup>  $\text{NO}_2$ , 2 vol.-%  $\text{CH}_4$  and 2 vol.-%  $\text{H}_2$ . Especially for toxic concentrations of ammonia and nitrogen dioxide or high concentrations of flammable gases, the developed sensor is suitable to prevent dangerous situations.

## 4.4 Temperature and humidity sensors on foil substrates

The foil-based temperature and humidity sensor development was carried out in three different stages: (1) development of the inkjet printing process based on sheet-to-sheet printing of sensor arrays, (2) optimization of the sensor layouts with sensor testing and (3) scaling of the printing process to roll-to-roll manufacture demonstration.

### 4.4.1 Printing process development

For the development of the inkjet process, laboratory printheads were used with tabletop printers. After this first stage, the compatibility of the developed silver and copper inks with industrial inkjet printheads was demonstrated (Figure 41).

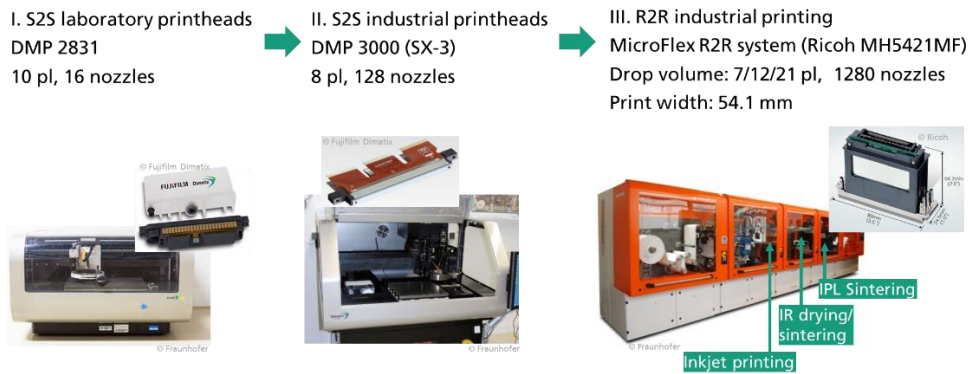


Figure 41: Development stages of inkjet printing process from S2S to R2R.

Figure 42 shows printed temperature and humidity sensors, printed with the developed silver ink (I50TM-119), after sintering at 150 °C for 30 min. The printed silver films show a good conductivity. The printed sensors resistance was near to the overall desired ohmic resistance of 100 Ohm or 1000 Ohm.

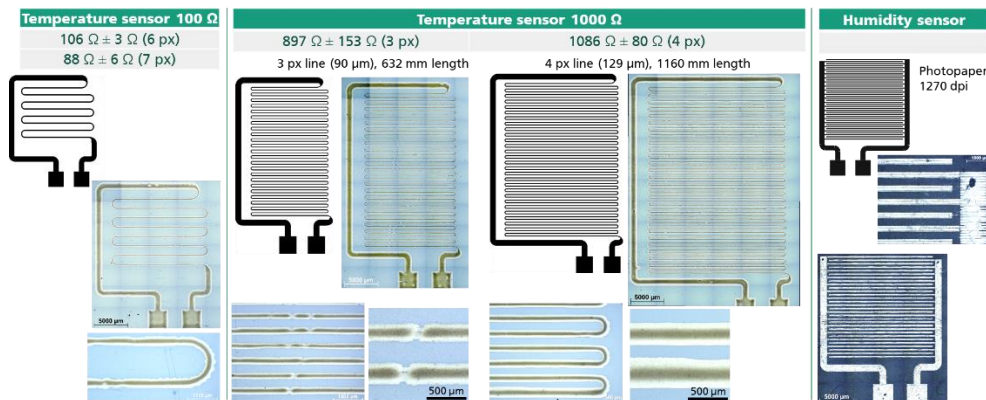


Figure 42: Inkjet printing of temperature sensors on PET and humidity sensors on paper foils.

A challenge for miniaturized print layouts is the avoidance of interrupted printed silver lines or short circuits between narrow printed neighbor lines. This is why the yield of repeatedly printed continuously conductive meanders of the sensor layouts was limited (Figure 43).

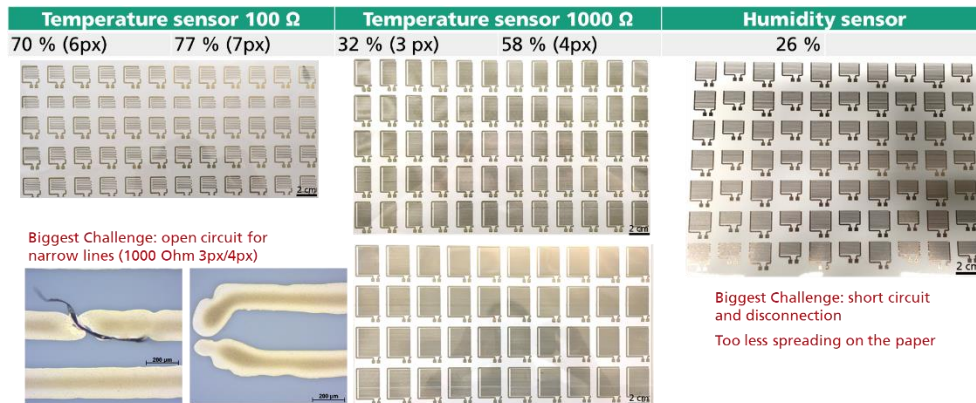


Figure 43: Inkjet printed sensor arrays and main challenges for miniaturized printing.

A reliable functioning of the individual printing nozzles as well as a reproducible and controlled ink wetting on the foil substrate are very important to achieve a high printing quality. Figure 44 gives some examples of typical issues of some line bulging and local constrictions as well as influence of nozzle misalignments during the printing process.

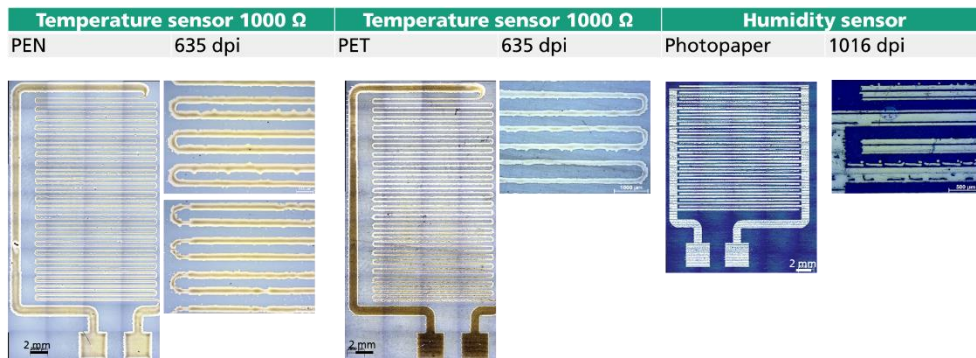


Figure 44: Typical issues during inkjet printing of silver ink on PEN, PET and paper foil substrates.

With optimization of the printing parameters, it was possible to demonstrate the inkjet printing compatibility of the project developed silver as well as copper inks on foil based substrates. The yield of continuously conductive sheet-to-sheet printed temperature sensors could be increased up to 88 %, which is rather good for a laboratory-based printing process (Figure 45).

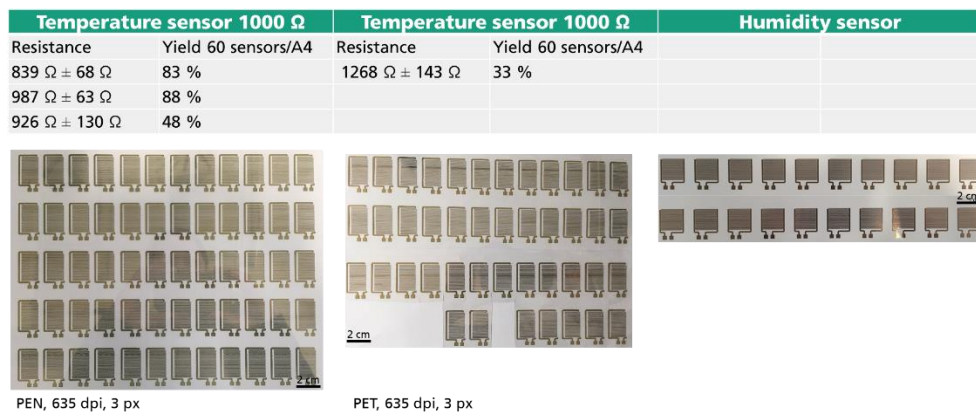


Figure 45: Inkjet printed sensors on PEN, PET and paper.



Optimal inkjet printing parameters were found for the I50TM-119 silver ink on PET substrate at 720 dpi print resolution and sintering at 130 °C for 30 min in a laboratory drying cabinet. The printed sensors were connected to copper wires for sensor testing. With sheet-to-sheet (S2S) printing a scaling of printed sensors to A4-sized PET sheets was demonstrated (**Figure 47**).

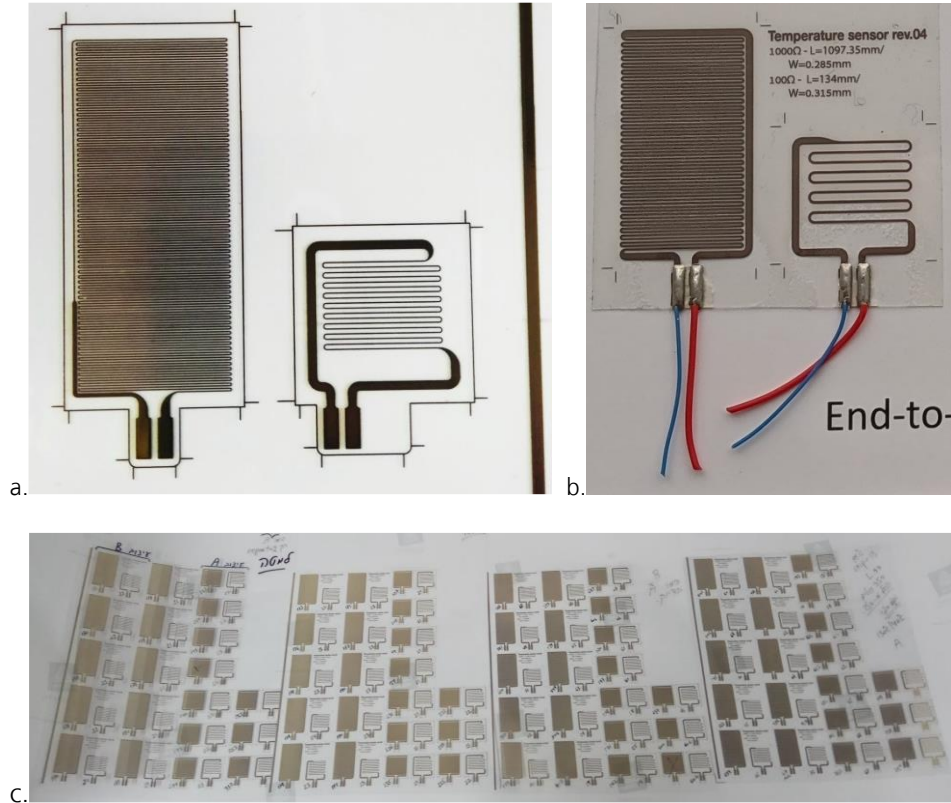


Figure 47: (a) 1000 Ohm and 100 Ohm temperature sensors printed on PET, (b) connecting the printed sensors for testing and (c) scaling of S2S inkjet printing of sensors.

The temperature sensors were tested in a climate chamber with a variation of the temperature between 10 °C to 90 °C at 50 % humidity (Figure 48). The printed 100 Ohm as well as 1000 Ohm sensors show good sensitivities and a reproducible correlation between temperature and resistance change, which directly corresponds to the temperature coefficient of resistance of the printed silver material.

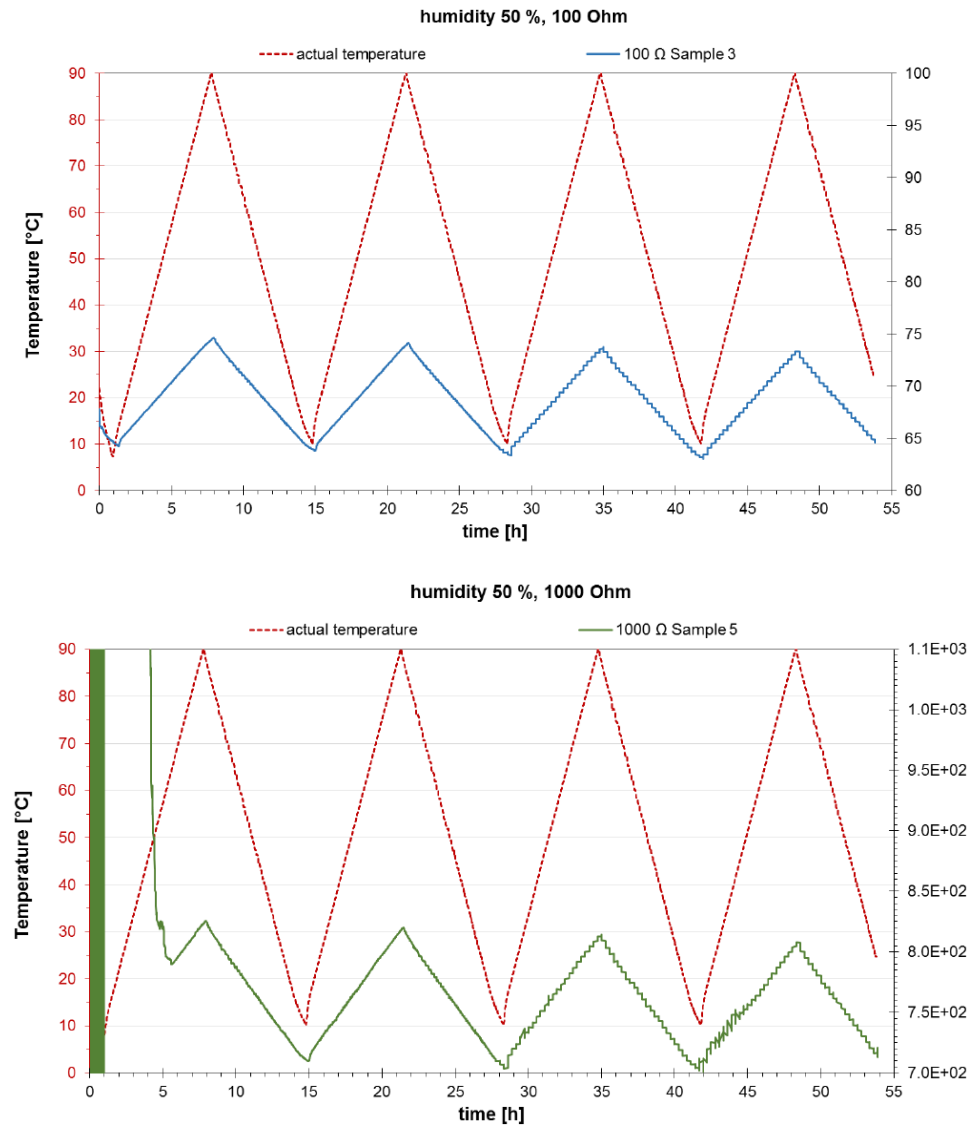


Figure 48: Temperature sensing test of inkjet printed sensors on PET foil.

### 4.4.3 Humidity sensor optimization and testing

For the humidity sensor an inkjet paper as substrate was chosen, since paper can easily interact and respond to humidity changes. A correlation between the paper humidity and resistance change of a printed interconnected silver electrode was evaluated. The printed films were sintered at 140 °C for 40 min. By optimizing the sensor layout (Figure 49), the resistance change, in respond to humidity changes of the paper substrate, were maximized.

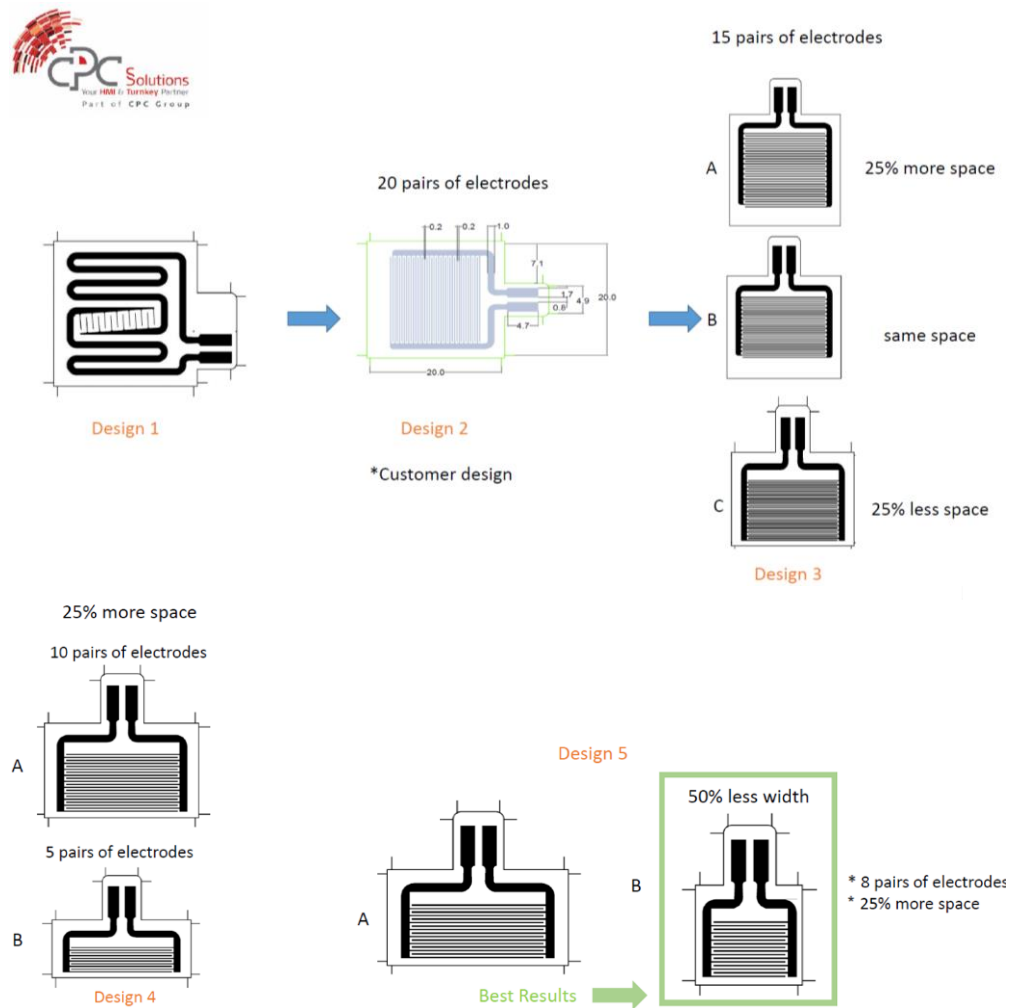


Figure 49: Evaluation of designs for an inkjet printed humidity sensor on paper substrate.

Figure 50 shows details of the silver printed interdigital electrode and the connecting of the humidity sensors to copper wires for testing.

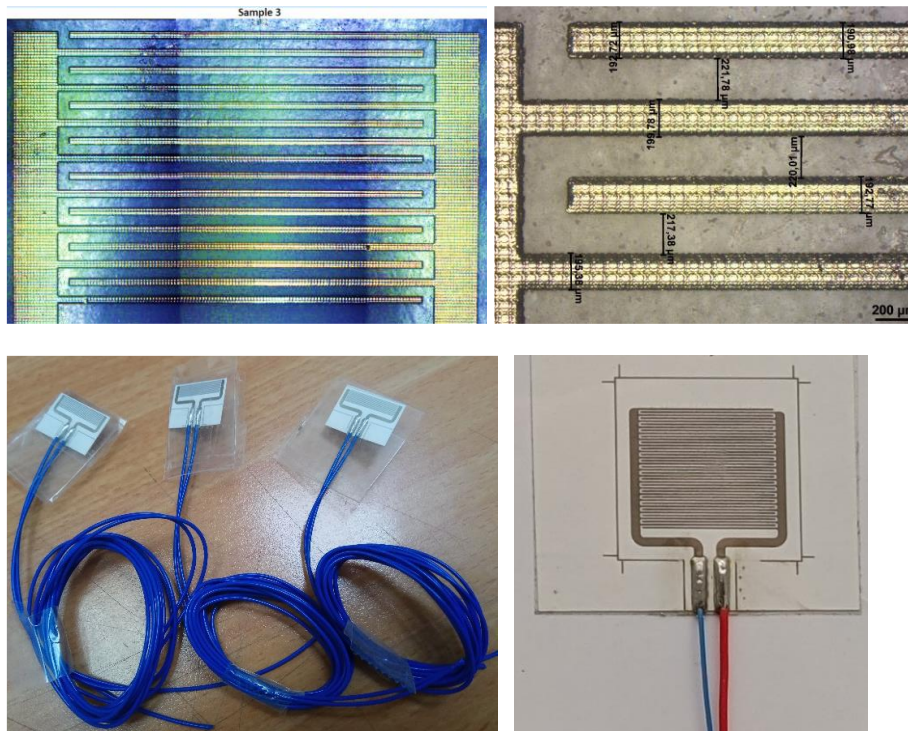


Figure 50: (top) Inkjet printed silver interdigital electrode of the humidity sensor on paper and (b) connecting the sensor to copper-wires for testing.

First humidity sensor tests in a climate chamber revealed a rather poor sensitivity to humidity changes. It was found that by applying a voltage to the interdigital electrode during measurement, the sensitivity of the sensor was increased significantly. By measurement of the sensor current, the calculation of the resistance change in dependence of the humidity was characterized. Functional printed humidity sensors were demonstrated for humidity ranges of 25 % to 75 % RH (Figure 51).

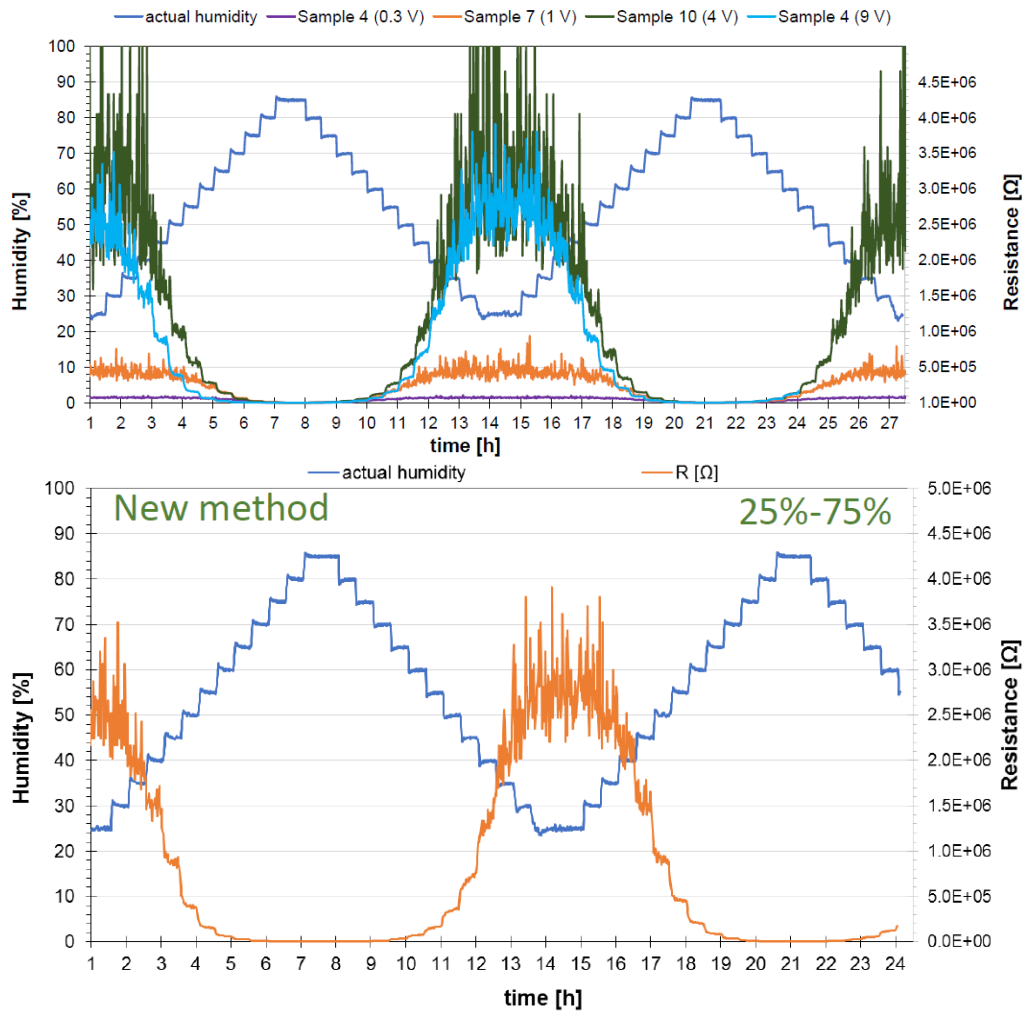


Figure 51: Testing of printed humidity sensors on paper substrate. (top) Evaluation of the influence of an applied sensing voltage on the sensor resistance and (bottom) optimized sensor with humidity sensitivity between 25 % to 75 % RH.

#### 4.4.4 Scaling of inkjet printed sensors to R2R

The scaling of the fabrication of inkjet printed temperature sensors on PET foil was demonstrated with a roll-to-roll (R2R) manufacturing machine (MicroFlex R2R machine, Figure 52). An industrial printhead from Ricoh MH5421MF with 1280 nozzles and a print width of 54.1 mm was used in single-pass printing at 600dpi. The printhead offers an ink recirculation, which improves the jetting stability and performance of the silver ink (I50TM-119).

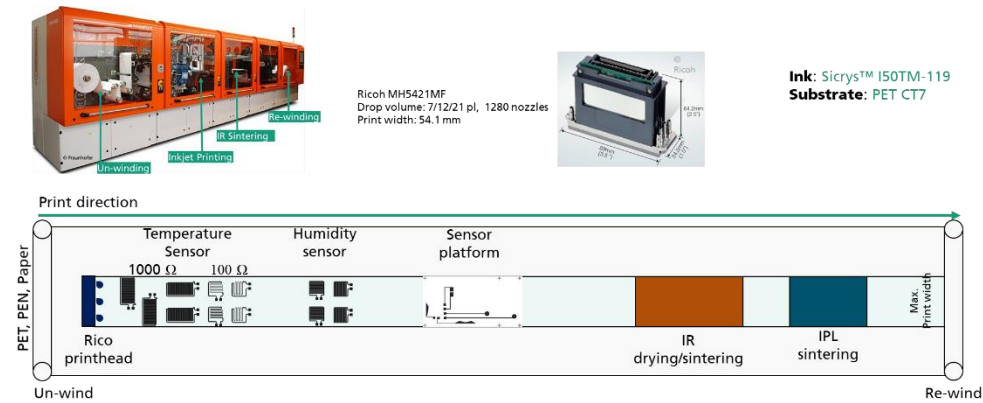


Figure 52: Roll-to-roll machine and set-up for inkjet printed sensors on flexible foils.

In Figure 53 details of the R2R machine like the PET foil un-winding, the inkjet printing unit, IR drying and sintering unit as well as the re-winding of the sensor printed PET foil is shown.

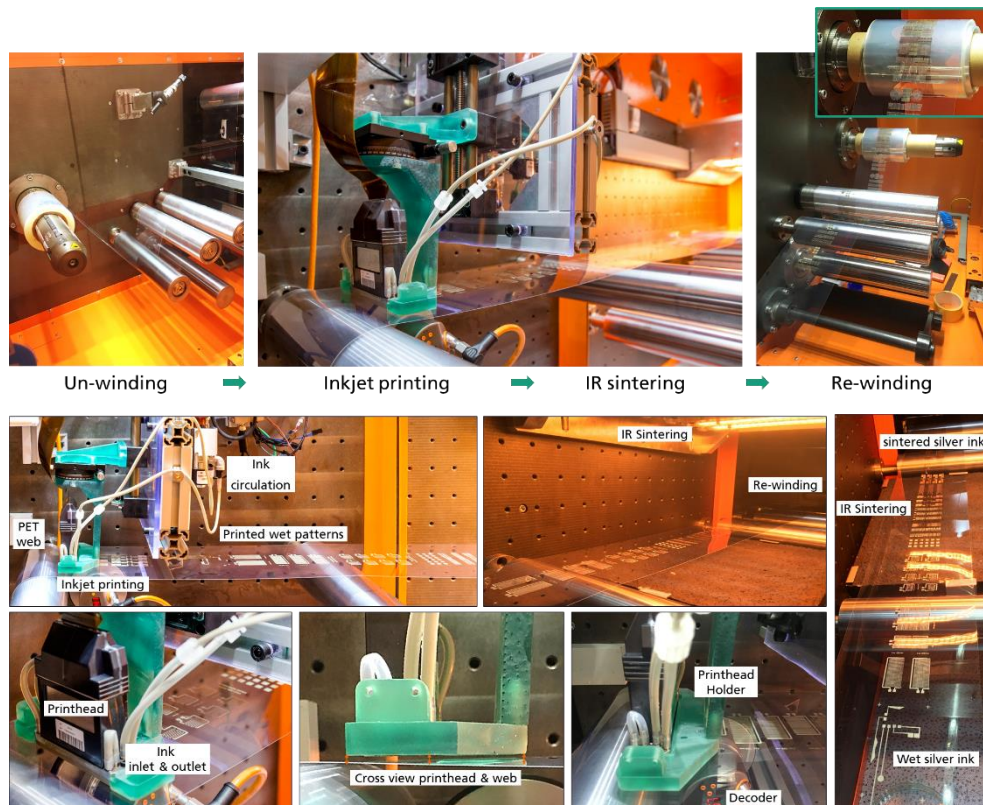


Figure 53: Details of the R2R inkjet printing machine (Microflex).

For the printing tests the printing speed and movement of the PET foil web was varied between 1 m/min, 2 m/min, 5 m/min, 10 m/min and up to 20 m/min. Even if the print-head can handle higher printing speeds by increasing the printing frequency, more print failures were observed for 5 m/min and above. Due to the limited length of the IR drying and sintering unit (50 cm) the max. speed for a complete ink sintering was limited to 2 m/min web movement.

Several print resolutions of 600/600 dpi, 900/600 dpi, 1200/600 dpi (x/y direction, in and perpendicular to web movement) were evaluated at 1 m/min web speed (Figure 54). Best printing results were found for 1200/600 dpi resolutions.

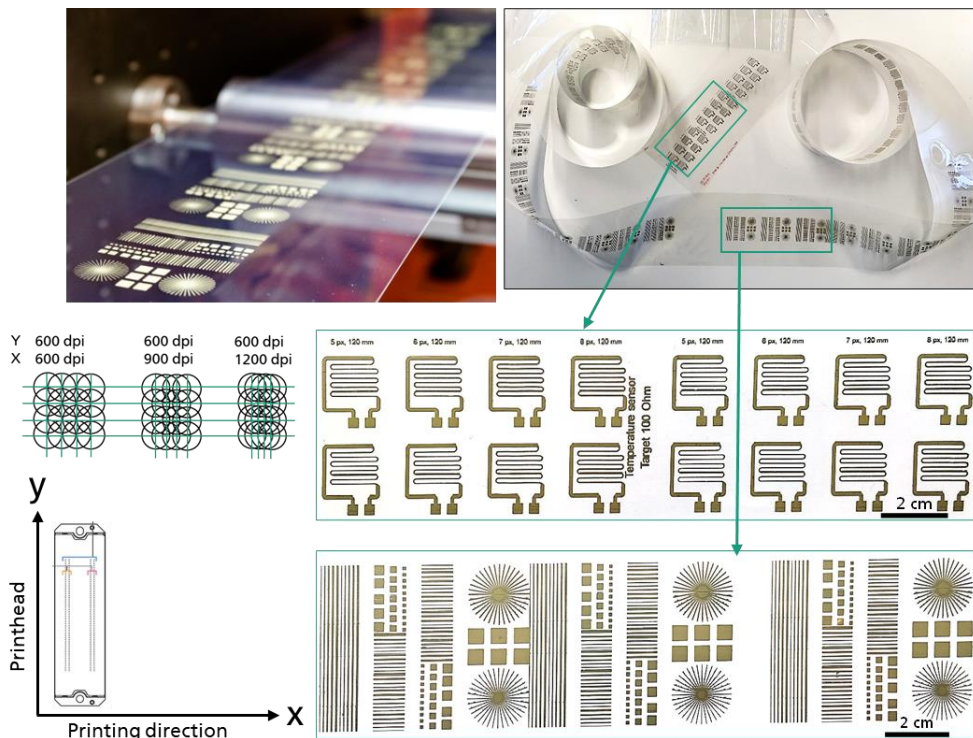


Figure 54: Quality control of R2R inkjet printed temperature sensors and test layouts [40].

Some challenges for the scaling in R2R printing were identified. With increasing web speed, some web vibrations occur, which change the distance between the print head nozzle and surface of the PET substrate. This effect can lead to some inaccuracies in positioning of single droplets in the print layout since the web is continuously moved underneath the print head. The industrial printhead has more than 1000 individual single nozzles, where some of them showed miss shooting or even nozzle failures. In a single pass printing process, this leads to inaccuracies or non-printing of individual droplets and pixels of the print layout (Figure 55). The occurrence of dust particles leads to isolated local failures in the printed films. At least the dried and sintered silver films are rather soft and by touching the rollers during web guiding and re-winding, scratches and surface impurities were visible on the printed sensor surface.

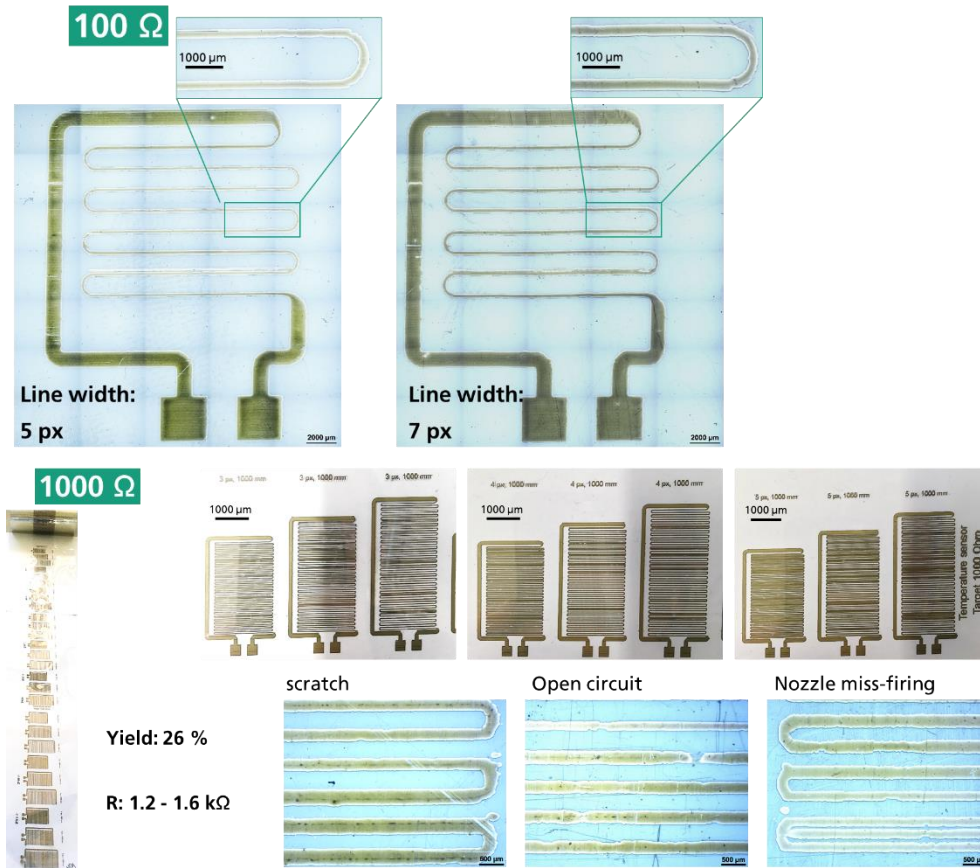


Figure 55: R2R inkjet printed temperature sensors with local print defects like non printed pixel and scratches due to roller handling.

The influence of the pixel width of the silver meander in the temperature sensor layout on the achievable yield during R2R printing as well as on the final sensor resistances was evaluated. With increased line width the yield of conductive sensors was increase from 63 % to 88 %. The corresponding sensor resistance decreases accordingly from 261 Ohm to 147 Ohm (**Table 14**).

**Table 14:** Influence of pixel width of sensor meander on yield and resistance.

px	Sensors [#]	Yield [%]	R [Ω]
5	10/16	63	261 ± 25 Ω
6	12/16	75	216 ± 26 Ω
7	12/16	75	168 ± 15 Ω
8	14/16	88	147 ± 13 Ω
<b>total</b>	<b>48/64</b>	<b>75</b>	

The sheet resistance of the single layer printed silver ink was  $0.5 \pm 0.02 \text{ } \Omega/\text{sq}$  at 1200/600 dpi printing resolution. With that a successful R2R inkjet printing of temperature sensors with  $147 \pm 13 \text{ } \Omega$  and 88 % yield was demonstrated. Further improvements in reduction of web vibrations, web straightness and surface cleaning along with an increased length of the IR drying and sintering unit, could improve further the overall achievable yield of such a R2R inkjet printing process.

## 4.5 Bluetooth sensor platform and RFID NFC sensor tag with printed antennas for wireless sensor communication

A 2.45 GHz low energy Bluetooth sensor platform was developed for wireless sensor communication within a 50 m radius. **Figure 56** shows the developed concept and the inkjet printed silver antenna as well as interconnects to the sensor, which can be attached to the Bluetooth board. The board can be powered by a battery with 1.7 V to 3.6 V (8.3 mA rectifying mode, 1  $\mu$ A standby). The powder of the amplifier for sending wireless signals is 8 dBm. A Si-chip is used to process the input impedance of the rectifier (31.4-j26.6 Ohm). The board is capable to handle 10 ADC ports and 4 analog input pins.

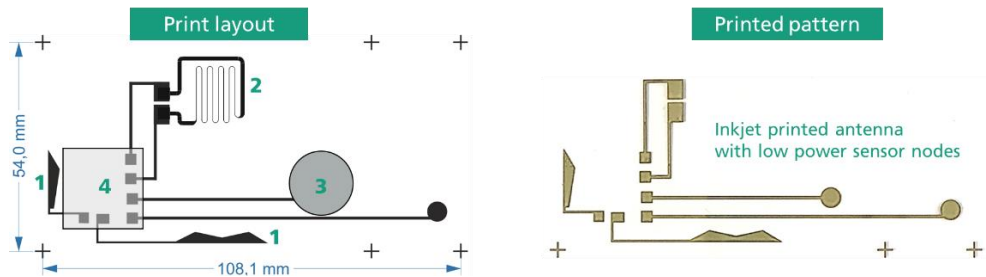


Figure 56: Low-energy Bluetooth board for wireless sensor communication.

The antenna was inkjet printed with the project developed silver ink (I50TM-119) on PET foil. The quality and parameters of the printed antenna are suitable for the desired application (Figure 57).

→ The wave impedance @ 2.45 GHz  
(69.8 - j15.6) $\Omega$  is close to the  
ideal case: (50 + j0) $\Omega$



→ The scattering parameter -13.9 dB  
@ 2.45 GHz → good antenna

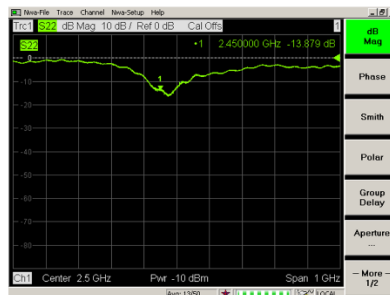


Figure 57: Characterization of a silver printed antenna on PET foil.

In a next step, the developed temperature sensor was attached to this Bluetooth board (Figure 58). Later, if this concept will be scaled to industrial manufacturing, the sensor by itself could directly be inkjet printed on this Bluetooth platform in parallel. Figure 58 shows the final Bluetooth platform with sensor, battery, printed antenna, interconnects and Si-chip.



Figure 58: Wireless low power sensor board with printed antenna: (1) 2.45 GHz antenna, (2) temperature sensor, (3) battery and (4) Bluetooth chip.

The wireless sensor communication was successfully demonstrated with a developed smartphone app (Figure 59). By simply touching the temperature sensor with hand, the increased temperature was monitored (25 – 33 °C).

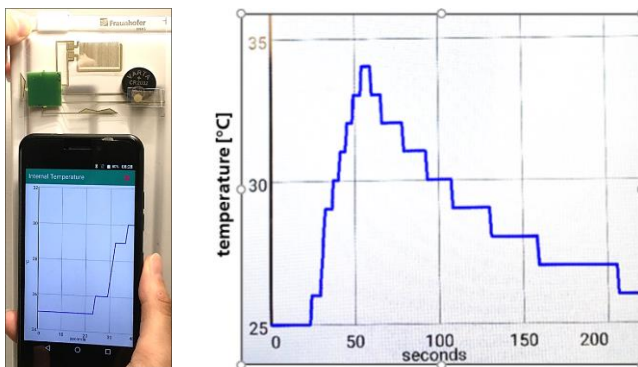


Figure 59: Demonstration of the wireless sensor communication based on the developed Bluetooth board, temperature sensor and smartphone app (Fraunhofer ENAS).

A **nearfield RFID NFC communication tag**, to digitally label individual sensors, was developed. The tag consists of a printed 13.56 MHz coil and an integrated RFID chip. To write or read information to this tag, the “NFC Tools PRO” with android phone was used.

Figure 60 shows the RFID tag concept and the silver inkjet printed coil on PET substrate.

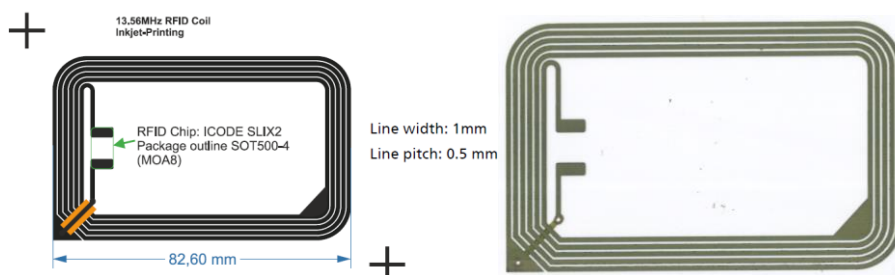


Figure 60: (left) Concept of a RFID NFC communication tag to digitally label sensors and (right) inkjet silver printed coil.

The inkjet printed coils were evaluated positively and showed a high inductance at a frequency of 13.56 MHz. The maximum readable distance between sample and reader

was determined to be 3.1 to 3.2 cm. For comparison, a standard RFID transponder shows a maximum readable distance of approx. 7 cm at comparable frequencies.

Table 15 summarizes the electrical properties of the inkjet printed silver coils on PET substrate.

Table 15: Characterization of inkjet printed silver coils for RFID sensor tags.

Printed coil sample	Impedance @ 13.56 MHz	Inductance @ 13.56 MHz
Coil 1 "73 Ω"	(72.9 +j321.8)Ω	3.8 μH
Coil 2 "79,2 Ω"	(79.6 +j316.3)Ω	3.7 μH
Coil 3 "82,8 Ω"	(82.3 +j316.1)Ω	3.7 μH

Finally, a RFID sensor tag demonstrator was prepared by attaching a commercial RFID chip to the printed coil. The overall sensor tag worked well and is ready for further industrial evaluation.

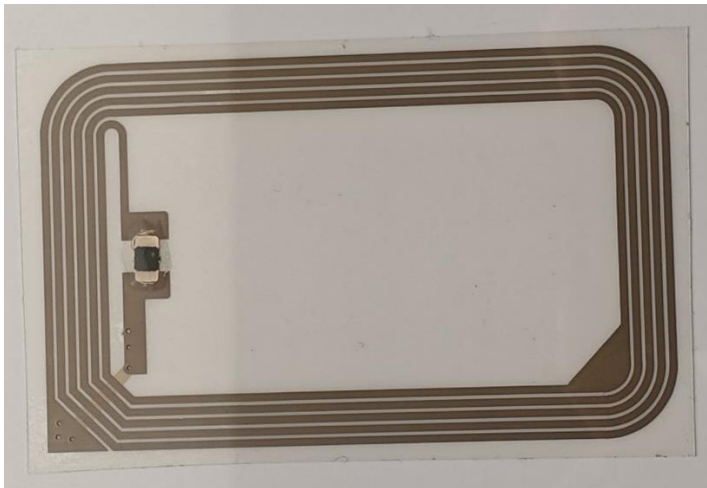


Figure 61: RFID sensor tag with integrated RFID chip, encapsulation adhesive and inkjet printed silver coil on PET foil.

## 5 Project publications

- M. Fritsch, S. Mosch, N. Trofimenko, M. Vinnichenko, M. Kusnezoff „Platinum nanoinks for inkjet printed sensors“, Poster, Printed Electronics Europe 2019 (IDTEchEx), 11.-12.04.2019 Berlin Germany, 2019.
- S. Kapadia, M. Fritsch, A. Kabla, F. M. Fuchs, E. Bilbao, L. Monsalve, J. Fossati, K. Y. Mitra, A. Trul, E. Agina, S. Ponomarenko, R. R. Baumann, “The Development & Fabrication of the All Inkjet Printed Electronic Devices using Novel Functional Materials Suitable for Various Sensing Applications in the Field of Printed and Flexible Electronic“, Oral Presentation, Printing for Fabrication 2019, San Fransisco, California, USA.
- M. Fritsch, S. Mosch, N. Trofimenko, V. Sauchuk, M. Vinnichenko, M. Kusnezoff, N. Beshchasna, M.S. Draz „Material inks for inkjet printed biomedical sensor applications“, Oral presentation and Poster, 30th Conference of the European Society for Biomaterials (ESB), 09.-13.09.2019, Dresden, Germany.
- N. Samotaev, K. Oblov, A. Gorshkova, M. Fritsch, S. Mosch, M. Vinnichenko, N. Trofimenko, M. Kusnezoff, F.M. Fuchs, L. Wissmeier „Ceramic microhotplates for low power metal oxide gas sensors“, Materials Today Proceedings, Vol. 30, Part 3, pp. 448-451, 2020. DOI: doi.org/10.1016/j.matpr.2019.12.394.
- N. Samotaev, K. Oblov, A. Gorshkova, M. Fritsch, S. Mosch, F.M. Fuchs, L. Wissmeier, M. Vinnichenko, N. Trofimenko, M. Kusnezoff „Ceramic microhotplates for low power metal oxide gas sensors“, International Scientific Conference “Materials Science: Composites, Alloys and Materials Chemistry” (MS-CAMC), St. Petersburg Russia, 20.-21.11.2019.
- N. Samotaev, K. Oblov, A. Ivanova, A. Gorshkova and B. Podlepetsky, "Rapid Prototyping of MOX Gas Sensors in Form-Factor of SMD Packages," 2019 IEEE 31st International Conference on Microelectronics (MIEL), Nis, Serbia, 2019, pp. 157-160, doi: 10.1109/MIEL.2019.8889576.
- M. Fritsch, S. Mosch, M. Vinnichenko, N. Trofimenko, M. Kusnezoff, F.M. Fuchs, L. Wissmeier, N. Samotaev, K. Oblov “Printed Miniaturized Platinum Heater on Ultra-Thin Ceramic Membrane for MOx Gas Sensors” ECS Meeting Abstracts, Vol.MA2020-01, IMCS 03: Electrochemical and Metal Oxide Sensors, 2020. DOI: 10.1149/MA2020-01282125mtgabs.
- M. Fritsch, S. Mosch, M. Vinnichenko, N. Trofimenko, M. Kusnezoff, F.-M. Fuchs, L. Wissmeier and N. Samotaev, “Printed miniaturized platinum heater on ultra-thin ceramic hotplates for low power semiconductive gas sensors“, Oral presentation, LOPEC conference (digital), 23.-25.03.2021.

The project results were presented at the following business fairs:

- Printed Electronics Europe 2019 (IDTEchEx), 11.-12.04.2019 Berlin Germany
- 30th Conference of the European Society for Biomaterials (ESB), 09.-13.09.2019, Dresden Germany.
- Printing for Fabrication 2019, 29.09.-03.10.2019 San Fransisco USA.

## 6 References

1. N. Barsan, D. Koziej, U. Weimar, *Sens. Actuators, B*, 121 (1), pp. 18-35 (2007).
2. <https://www.figaro.co.jp/en/product/sensor/>
3. <https://www.sensirion.com/en/environmental-sensors/gas-sensors/>
4. <https://www.sgxsensortech.com/products-services/industrial-safety/metal-oxide-sensors/>
5. <https://www.winsen-sensor.com/sensors/mems-gas-sensor/>
6. J. Van Den Broek, A.T. Güntner, S.E. Pratsinis, *ACS Sens.*, 3 (3), pp. 677-683 (2018).
7. N. Samotaev, A. Litvinov, M. Etrekova, K. Oblov, D. Filipchuk, A. Mikhailov, *Sensors (Switzerland)*, 20 (5), article № 1514 (2020).
8. J. Van Den Broek, S. Abegg, S.E. Pratsinis, A.T. Güntner, *Nat. Commun.*, 10 (1), 4220 (2019).
9. M. Leidinger, M. Rieger, T. Sauerwald, C. Alépée, A. Schütze, *Sens. Actuators, B*, 236, pp. 988-996 (2016).
10. A. Kock, R. Wimmer-Teubenbacher, F. Sosada-Ludwikowska, K. Rohrer, E. Wachmann, M. Herold, T.V. Welden, J. Min Kim, Z. Ali, A. Poenninger, M. Stahl-Offergeld, H.-P. Hohe, J. Lorenz, T. Erlbacher, G. Dolmans, P. Offermans, M. Vandecasteele, O. Yurchenko, O. Von Sicard, R. Pohle, F. Udrea, C. Falco, D. Flandre, D. Bol, E. Comini, D. Zappa, J. Gardner, M. Cole, J. Theunis, J. Peters, A. Baldwin, 2019 20th International Conference on Solid-State Sensors, Actuators and Microsystems and Eurosensors XXXIII, TRANSDUCERS 2019 and EUROSENSORS XXXIII, pp. 1136-1139 (2019)
11. <https://www.idt.com/us/en/document/dst/zmod4410-datasheet>
12. <https://www.bosch-sensortec.com/media/boschsensortec/downloads/datasheets/bst-bme680-ds001.pdf>
13. S. Dietrich, M. Kusnezoff, N. Trofimenko, W. Beckert, J. Henze, *Dresdner Sensor-Symposium*, pp.219-223 (2013).
14. A.A. Vasiliev, A.V. Pisiakov, A.V. Sokolov, N.N. Samotaev, S.A. Soloviev, K. Oblov, V. Guarnieri, L. Lorenzelli, J. Brunelli, A. Maglione, A.S. Lipilin, A. Mozalev, A.V. Legin, *Sens. Actuators, B*, 224, pp. 700-713 (2016).
15. [https://www.kerafol.com/\\_wpframe\\_custom/downloads/files/KERAFOL\\_Datenblatt\\_3YSZ\\_01-20\\_\\_081212-20022020.pdf](https://www.kerafol.com/_wpframe_custom/downloads/files/KERAFOL_Datenblatt_3YSZ_01-20__081212-20022020.pdf)
16. [https://www.kerafol.com/\\_wpframe\\_custom/downloads/files/KERAFOL\\_Datenblatt\\_Keral96\\_01-20\\_\\_081306-20022020.pdf](https://www.kerafol.com/_wpframe_custom/downloads/files/KERAFOL_Datenblatt_Keral96_01-20__081306-20022020.pdf)
17. [https://www.ikts.fraunhofer.de/en/departments/energy\\_systems/materials\\_and\\_components/HT\\_ElectrochemistryCatalysis/material\\_inks.html](https://www.ikts.fraunhofer.de/en/departments/energy_systems/materials_and_components/HT_ElectrochemistryCatalysis/material_inks.html)
18. <https://www.pvnanocell.com/silver-inks.html>
19. N.N. Samotaev, A.A. Vasiliev, B.I. Podlepetsky, A.V. Sokolov, A.V. Pisiakov, *Sens. Actuators, B*, 127 (1), pp. 242-247 (2007).
20. N. Samotaev, K. Oblov, M. Etrekova, D. Veselov, A. Gorshkova, *Materials Science Forum*, 977, pp. 238-243 (2020).
21. E. Sowade, K.Y. Mitra, E. Ramon, C. Martínez-Domingo, F. Villani, F. Loffredo, H. L. Gomes, R.R. Baumann "Up-scaling of the manufacturing of all-inkjet-printed organic thin-film transistors: Device performance and manufacturing yield of transistor ar-rays", *Organic Electronics*, Vol. 30, pp. 237-246, 2016. DOI: 10.1016/j.orgel.2015.12.018.

22. C. Gaspar, J. Olkkonen, S. Passoja and M. Smolander "Paper as Active Layer in Inkjet-Printed Capacitive Humidity Sensors", *Sensors*, 17(7), 1464, 2017. DOI: doi.org/10.3390/s17071464.
23. P. Teunissen et al. „Industrial scale production of RFID devices by roll-to-roll inkjet printing of conductive inks“, IJC Düsseldorf Germany, September 30, 2014. [https://www.researchgate.net/publication/267507442\\_Industrial\\_scale\\_production\\_of\\_RFID\\_devices\\_by\\_roll-to-roll\\_inkjet\\_printing\\_of\\_conductive\\_inks](https://www.researchgate.net/publication/267507442_Industrial_scale_production_of_RFID_devices_by_roll-to-roll_inkjet_printing_of_conductive_inks).
24. S. Khan et al. "Recent Developments in Printing Flexible and Wearable Sensing Electronics for Healthcare Applications", *Sensors*, 19, 1230, 2019, DOI 10.3390/s19051230.
25. K. Xu et al. "Multifunctional Skin-Inspired Flexible Sensor Systems for Wearable Electronics", *Adv.Mater.Technol.*, 4, 1800628, 2019, DOI 10.1002/admt.201800628.
26. K. Takei et al. „Physical and Chemical Sensing With Electronic Skin“, *Proceedings of IEEE*, pp.1-13, 2019, DOI: 10.1109/JPROC.2019.2907317.
27. B. Polzinger „Inkjetdruck von Silberleiterbahnen zur Anwendung als Temperatur-sensor“ Dissertation Universität Stuttgart, ISBN 978-3-8439-3483-, 2017.
28. J. Keck, B. Freisinger, D. Juric, K. Gläser, M. Völker, W. Eberhardt, A. Zimmermann "Low-Temperature Sintering of Nanometal Inks on Polymer Substrates" 13th International Congress Molded Interconnect Devices (MID), Würzburg, 2018, pp. 1-7, Doi 10.1109/ICMID.2018.8527053.
29. Kamyshny, A.; Magdassi, S. Conductive nanomaterials for printed electronics. *Small* 2014, 10, 3515–3535.
30. Kamyshny, A.; Magdassi, S. Aqueous dispersions of metallic nanoparticles: preparation, stabilization and application. *Nanoscience: Colloidal and Interfacial Aspects* 2010, 747–778.
31. Szczech, J.; Megaridis, C.; Zhang, J.; Gamota, D. Ink jet processing of metallic nanoparticle suspensions for electronic circuitry fabrication. *Microscale Thermophysical Engineering* 2004, 8, 327–339.
32. Magdassi, S.; Grouchko, M.; Berezin, O.; Kamyshny, A. Triggering the sintering of silver nanoparticles at room temperature. *ACS nano* 2010, 4, 1943–1948.
33. Cummins, G.; Desmulliez, M. P. Inkjet printing of conductive materials: a review. *Circuit World* 2012, 38, 193–213.
34. <https://www.dupont.com/electronic-materials/printed-electronics.html>
35. <https://www.pvnanocell.com/>
36. <https://www.novacentrix.com/products/metalon-conductive-inks>
37. [https://www.ikts.fraunhofer.de/en/departments/energy\\_systems/materials\\_and\\_components/HT\\_ElectrochemistryCatalysis/material\\_inks.html](https://www.ikts.fraunhofer.de/en/departments/energy_systems/materials_and_components/HT_ElectrochemistryCatalysis/material_inks.html)
38. M. Zea, A. Moya, M. Fritsch, E. Roman, R. Villa, G. Gabriel "Enhanced performance stability of iridium oxide based pH sensors fabricated on rough inkjet-printed platinum", *Journal of Applied Materials and Interfaces*, 11, 16, pp.15160-15169. 2019. DOI: doi.org/10.1021/acsami.9b03085.
39. I. A. Volkov et al. "Platinum based nanoparticles produced by a pulsed spark discharge as a promising material for gas sensors", *Appl. Sci.*, 11, 526, 2021. DOI: doi.org/10.3390/app11020526.
40. D. Mitra et al., publication planned / in press.

## 7 Tables

Table 1: Steps for the gas sensor fabrication.

.....  
13

Table 2: Specification of the printed films for the gas sensor.

.....  
15

Table 3: Targets of gas detection limits of the gas sensor.

.....  
15

Table 4: Specification of the printed films for the temperature and humidity sensors.

.....  
16

Table 5: Specification of the printed temperature and humidity sensors.

.....  
16

Table 6: Properties of developed silver inks.

.....  
18

Table 7: Properties of developed silver ink "I50TM-119" (\* contact angle by OWRK method, \*\* ISO 2409 Standard without cuts).

.....  
18

Table 8: Properties of developed copper inks.

.....  
19

Table 9: MOx ink materials for gas sensing.

.....  
23

Table 10: Ceramic substrate processing parameters.

.....  
24

Table 11: Zirconia substrate material.

.....  
25

Table 12: HPDL laser sintering of printed heater with Pt-glass-inks.

.....  
29

Table 13: Parameters of developed gas sensor demonstrator.

.....  
35

Table 14: Influence of pixel width of sensor meander on yield and resistance.

.....  
48

Table 15: Characterization of inkjet printed silver coils for RFID sensor tags.

.....  
51

## 8 Figures

Figure 1: Process flow of gas sensor preparation.

.....  
13

Figure 2: (top) Layout of printed platinum electrode and heater on a thin free-cut zirconia membrane and (bottom) integration of the membrane in a ceramic gas sensor package.

.....  
14

Figure 3: (left) Arrangement of the heater on the zirconia membrane and (right) miniaturized platinum heater layout.

.....  
14

Figure 4: Principle layout of temperature (left) and humidity sensor (right).

.....  
15

Figure 5: Low Energy Bluetooth sensor communication platform with chip "BLUENRG2" by ST (Fraunhofer ENAS).

.....  
16

Figure 6: Nearfield RFID NFC communication tag for digital sensor labeling.

.....  
17

Figure 7: (left) Synthesized silver (mean particle size of 70nm) and (right) copper particles (mean particle size of 50 nm).

.....  
17

Figure 8: Silver ink "I50TM-119" on Kapton foil. (left) After printing and drying and (right) after sintering and 180 ° bending test.

.....  
18

Figure 9: Printed copper ink "IC40DM-7" films on PET and Kapton polymer foils.

.....  
19

Figure 10: Laser sintering of inkjet printed copper films on PET and Kapton.

.....  
19

Figure 11: Strategy for the platinum ink development.

.....  
20

Figure 12: Synthesized platinum particles for the ink formulation (mean particle size of 50 nm).

.....  
20

Figure 13: (top) Particle size distribution of a 20 wt.-% platinum ink and (bottom) sedimentation behavior of the ink in a centrifugal field (both measured by Lumiziser).

.....  
21

Figure 14: Main issues during the platinum ink development.  
 .....  
 22

Figure 15: Comparison of aerosol-jet printed and dried Pt-films on zirconia substrate based on (left) water based ink solvent and (right) water-free ink solvent (bottom pictures show the wetting of the ink solvent carrier).  
 .....  
 22

Figure 16: (left) Glass powder after intensive high-energy milling procedure with particle size below 200 nm and (right) cross section of a sintered Pt-glass-composite-ink on zirconia with formation of a glass adhesion layer.  
 .....  
 23

Figure 17: Workflow for zirconia substrate development.  
 .....  
 24

Figure 18: Zirconia (3YSZ) substrates with 40  $\mu\text{m}$  (left, middle) and 30  $\mu\text{m}$  thickness (right).  
 .....  
 24

Figure 19: (left) optical inspection system and (right) examples of defect classification.  
 .....  
 25

Figure 20: Fujifilm Dimatix inkjet printer DMP-2831 with 10 pl print head.  
 .....  
 26

Figure 21: Inkjet printed platinum heater on zirconia substrate.  
 .....  
 26

Figure 22: Aerosol-jet printer M3D from Optomec, USA.  
 .....  
 26

Figure 23: Aerosol-jet printed platinum heater on zirconia after drying.  
 .....  
 27

Figure 24: (top) Printed heater based on Pt-glass-ink after drying at 80  $^{\circ}\text{C}$  and (bottom) heater after sintering at 760  $^{\circ}\text{C}$  in a muffle furnace.  
 .....  
 27

Figure 25: SEM analysis of printed platinum films after drying and sintering in a furnace.  
 .....  
 28

Figure 26: High-power diode laser sintering (HPDL) of printed films.  
 .....  
 28

Figure 27: SEM analysis of the surface microstructure of a HPDL sintered platinum-glass film on zirconia.  
 .....  
 29

Figure 28: (left) XRF analysis of printed platinum heaters with (right) correlation of the platinum mass per unit area to the heater resistance after laser sintering.  
 .....  
 29

Figure 29: Set-up for platinum heater test (printed on 90  $\mu\text{m}$  thick zirconia) with contacting and IR camera equipment.

30  
Figure 30: (left) Sputtered Pt-heater on 50 µm zirconia membrane (free-cut hot-plate of 280 µm size) and (right) power consumption tests.

30  
Figure 31: Array of sensor chips of 30 µm thin zirconia prepared by laser micro-milling.

31  
Figure 32: Integration of an ink-jet printing tool with a laser micro-milling system: (1) laser scanner with integrated hardware; (2) graphical interface of the implemented 4-coordinate laser micro-processing control software; (3) displayed image of milled area from a microscope with amplifying up to 2000 times; (4) constantly displayed camera image to monitor the processing area; (5) XQR41 Series Traditional Pneumatic Valve kit with 150 µm dot diameter ; (6) PICO jet valve set with 50 micron nozzle.

31  
Figure 33: Ceramic MOX gas sensor housing in a SOT-23 package form-factor with dimension 1.4 × 3.0 × 1.00 mm.

32  
Figure 34: Scaling of micro-milling fabrication of MOX sensor packages and zirconia hot-plates.

33  
Figure 35: (top left) Floating effect of a sensor package with silver ink metallization in a soldering paste; (top right) soldered sensor package with flux; (bottom) gas sensor assembled in TO-8 package by using a standard PCB with ENIG coating.

33  
Figure 36: Gas sensor testing equipment (Mephi and RIIT).

34  
Figure 37: MOX gas sensor demonstrator (RIIT).

35  
Figure 38: Pre-aging of MOX gas sensors on a demonstrator electronic module (RIIT).

36  
Figure 39: Dependence of the sensor signal resistance from the supply voltage.

36  
Figure 40: Gas sensing test of the developed MOX gas sensor.

37  
Figure 41: Development stages of inkjet printing process from S2S to R2R.

38  
Figure 42: Inkjet printing of temperature sensors on PET and humidity sensors on paper foils.

38

Figure 43: Inkjet printed sensor arrays and main challenges for miniaturized printing.  
 .....  
 39

Figure 44: Typical issues during inkjet printing of silver ink on PEN, PET and paper foil substrates.  
 .....  
 39

Figure 45: Inkjet printed sensors on PEN, PET and paper.  
 .....  
 39

Figure 46: Evaluation of temperature sensor designs.  
 .....  
 40

Figure 47: (a) 1000 Ohm and 100 Ohm temperature sensors printed on PET, (b) connecting the printed sensors for testing and (c) scaling of S2S inkjet printing of sensors.  
 .....  
 41

Figure 48: Temperature sensing test of inkjet printed sensors on PET foil.  
 .....  
 42

Figure 49: Evaluation of designs for an inkjet printed humidity sensor on paper substrate.  
 .....  
 43

Figure 50: (top) Inkjet printed silver interdigital electrode of the humidity sensor on paper and (b) connecting the sensor to copper-wires for testing.  
 .....  
 44

Figure 51: Testing of printed humidity sensors on paper substrate. (top) Evaluation of the influence of an applied sensing voltage on the sensor resistance and (bottom) optimized sensor with humidity sensitivity between 25 % to 75 % RH.  
 .....  
 45

Figure 52: Roll-to-roll machine and set-up for inkjet printed sensors on flexible foils.  
 .....  
 46

Figure 53: Details of the R2R inkjet printing machine (Microflex).  
 .....  
 46

Figure 54: Quality control of R2R inkjet printed temperature sensors and test layouts [40].  
 .....  
 47

Figure 55: R2R inkjet printed temperature sensors with local print defects like non printed pixel and scratches due to roller handling.  
 .....  
 48

Figure 56: Low-energy Bluetooth board for wireless sensor communication.  
 .....  
 49

Figure 57: Characterization of a silver printed antenna on PET foil.  
 .....  
 49

Figure 58: Wireless low power sensor board with printed antenna: (1) 2.45 GHz antenna, (2) temperature sensor, (3) battery and (4) Bluetooth chip.  
.....  
50

Figure 59: Demonstration of the wireless sensor communication based on the developed Bluetooth board, temperature sensor and smartphone app (Fraunhofer ENAS).  
.....  
50

Figure 60: (left) Concept of a RFID NFC communication tag to digitally label sensors and (right) inkjet silver printed coil.  
.....  
50

Figure 61: RFID sensor tag with integrated RFID chip, encapsulation adhesive and inkjet printed silver coil on PET foil.  
.....  
51